UNESCO Chair on
Coastal Geo-Hazard Analysis
Research Institute for Earth Sciences
Geological Survey of Iran
unesco
Chair

Abstract

The evaluation of seismic potential of the Astara fault, with a length of about 110 km and considering the residence of more than 150.000 people within the fault zone, is of great importance. The Astara fault with a general N-S trend, is located on the eastern border of Talesh Mountains. Hitherto, the largest earthquake (Mw 6.6) in this vicinity has been recorded at a distance of 15km from the Astara fault.

Geometrically, the Astara fault as an active fault zone, kinematically could be distinguished as a wide zone consists of two major faults: (1) Astara thrust fault (ATF) which is located close to the mountain range. (2) Active Astara strike-slip fault (ASF).

Measured maximum and minimum horizontal displacements along the fault are 1500 m and 70 m respectively, and maximum and minimum vertical displacements are 130 m and 5 m respectively. Present estimated rake value is 0 to 12 towards SW with a slip rate ~ 1.5 mm/yr. On the basis of Paleoseismological investigations in Lisar Trench, and using C^{14} age determinations, it is evident that at least 3 to 4 Paleoearthquakes with magnitudes Mw 6.24-5.74 occurred around 30.000 year ago, and based on the sedimentation rated of trench layers, the estimated magnitude of the youngest (~ 5.000 yrs.) and oldest (~30.000 yrs.) events are Mw 6.24 and Mw 5.74 respectively.

ISBN : 978-622-8423-12-8

2024

unesco
Chair
UNESCO Chair on
Coastal Geo-Hazard Analysis
Research Institute for Earth Sciences
Geological Survey of Iran

UNESCO Chair on
Coastal Geo-Hazard Analysis
Research Institute for Earth Sciences
Geological Survey of Iran
unesco
Chair

Paleoseismological investigations along the Astara fault system

UCCGHA 024

2024

Paleoseismological investigations along the Astara fault system

سرشناسه	:	نوروزی، ملیحه، ۱۳۶۷- -Nowrouzi, Maliheh, 1989
عنوان و نام پدیدآور	:	Paleoseismological investigations along the Astara fault system[Book]/ author Maliheh Nowrouzi; supervisors Hamid Nazari, Manouchehr Ghorashi, Mohammad Ali Shokri; employer Research Institute for Earth Sciences, Geological survey of Iran; with cooperation UNESCO Chair on Coastal Geo-Hazard Analysis.
مشخصات نشر	:	تهران: نشر خزه، ۱۴۰۳= ۲۰۲۴م.
مشخصات ظاهری	:	ه، ۱۰۲ ص.: مصور(رنگی)، نمودار.
شابک	:	978-622-8423-12-8
وضعیت فهرست نویسی	:	فیپا
یادداشت	:	زبان: انگلیسی.
یادداشت	:	عنوان به فارسی: بررسی‌های پارینه لرزه‌شناسی بر روی گسل آستارا
یادداشت	:	کتابنامه:ص. ۱۰۲.
آوانویسی عنوان	:	پالئوسایزمولوژی
موضوع	:	گسله‌ها -- آستارا -- ایران
موضوع	:	Faults (Geology) -- Astara -- Iran
موضوع	:	دیرینه لرزه شناسی
موضوع	:	Paleoseismology
شناسه افزوده	:	نظری، حمید، ۱۳۴۶-، ناظر
شناسه افزوده	:	Nazari, Hamid, 1968-
شناسه افزوده	:	قرشی، منوچهر، ۱۳۲۰-، ناظر
شناسه افزوده	:	Ghorashi, Manouchehr, 1941
شناسه افزوده	:	شکری، محمدعلی، ۱۳۵٦-، ناظر
شناسه افزوده	:	Shokri, Mohammad Ali, 1977-
شناسه افزوده	:	یونسکو. کرسی مخاطرات زمین شناختی ساحلی
شناسه افزوده	:	UNESCO Chair on Coastal Geo-Hazard Analysis
شناسه افزوده	:	سازمان زمین‌شناسی و اکتشافات معدنی کشور. پژوهشکده علوم زمین
شناسه افزوده	:	Geological Survey of Iran. Research Institute for Earth Sciences
رده بندی کنگره	:	QE۵۳۷//۲ب۴پ۲ ۱۴۰۳
رده بندی دیویی	:	۲۲۰۹۵۵۲۳۶۶/۵۵۱
شماره کتابشناسی ملی	:	۹۷۲۲۷۸۱

Paleoseismological investigations along the Astara fault system

Author:

Maliheh Nowrouzi

نشرخزه

اطلاعات گزارش

عنوان: بررسی‌های پارینه‌لرزه‌شناسی بر روی گسل آستارا
مجری: پژوهشکده علوم زمین، سازمان زمین‌شناسی و اکتشافات معدنی کشور
زبان مرجع: فارسی
خروجی: گزارش، نقشه، مقاله، داده های الکترونیکی
ناظران علمی: حمید نظری، منوچهر قرشی، محمدعلی شکری
نویسندگان: ملیحه نوروزی
رئیس کرسی یونسکو در مخاطرات زمین شناختی ساحلی: حمید نظری
مسئول شورای اجرایی: راضیه لک
خلاصه‌نویسی و ترجمه به انگلیسی: منوچهر قرشی
خلاصه شده از: طرح مخاطرات زمین شناسی دریایی حوضه جنوب کاسپین
ناشر: نشر خزه
با همکاری کرسی یونسکو در مخاطرات زمین شناختی ساحلی
چاپ اول: ۱۴۰۳
شمارگان: ۵۰ نسخه
صفحات: ۱۰۲
شابک: ۸-۱۲-۸۴۲۳-۶۲۲-۹۷۸
khazepub@gmail.com

Report Information

Title: Paleoseismological investigations along the Astara fault system

Employer: Research Institute for Earth Sciences, Geological survey of Iran

Original language: Persian

Output: Report, Map, Paper, Digital Meta Data

Supervisors: Hamid Nazari, Manouchehr Ghorashi, Mohammad Ali Shokri

Authors: Maliheh Nowrouzi

Chairholder in the UNESCO Chair on Coastal Geo-Hazard Analysis: Hamid Nazari

Head of the Executive Council: Razyeh Lak

Summarized and translated into English: Manouchehr Ghorashi

Summarized after: Geohazard South Caspian Carpet (GSCC)

Publisher: Khazeh Publication

with cooperation UNESCO Chair on Coastal Geo-Hazard Analysis

First Edition: 2024

Edition number: 50

Page: 162

Shabak: 978-622-8423-12-8

khazepub@gmail.com

Scientific Council

Name	Affiliation
Ara Avagyan	IGS: Institute Geological Sciences
Rick J Bailey	IOC-UNESCO Indian Ocean Tsunami Warning and Mitigation System/ UNESCO
Aram Fathian Baneh	University of Calgary
Wenjiao Xiao	Chinese Academy of Sciences
Magdi Guirguis	Institut français d'archéologie orientale du Caire
Richard Walker	University of Oxford
Philippe Agard	University of Sorbonne
Justin Ahanhanzo	Intergovernmental Oceanographic Commission of UNESCO (IOC-UNESCO)
Alice Aurelie	UNESCO Water Sciences Division
Eric Barrier	University of Sorbonne
Jean-François Ritz	University of Montpellier
Martin Hanz	German under water archaeology association
Klaus Reicherter	Aachen University
Judith Thomalsky	German Archaeological Institute Tehran Branch
Hamid Alizadeh Lahijani	Iranian National Institute for Oceanography and Atmospheric

	Science
Abbas Banj Shafiei	Urmia University
Yahya Djamour	Shahid Beheshti University (SBU)
Behrouz Abtahi	Shahid Beheshti University (SBU)
Hassan Fazeli Nashli	University of Tehran
Razyeh Lak	Research Institute for Earth Sciences
Mohammad Mokhtari	International Institute of Earthquake Engineering and Seismology
Hamid Nazari	Research Institute for Earth Sciences
Jafar Omrani	Geological Survey of Iran
Morteza Talebian	Research Institute for Earth Sciences
Mohammad Tatar	International Institute of Earthquake Engineering and Seismology
Alireza Zarasvandi	Iranian Research Organization for Science & Technology (IROST) – Ministry of Science, Research & Technology
Mahdi Zare	International Institute of Earthquake Engineering and Seismology
Stefano Salvi	National Institute of Geophysics and Volcanology (INGV)
Ryo Anma	Tokushima University
Yeong Bae Seong	Korea University
John Lambert	Deltares, UNESCO
Issa El-Hussain	Sultan Qaboos University

Ekkehard Holzbecher	German University of Technology in Oman
Egor Krasinskiy	Underwater research center Russian Geographical Society
Audemard Franck A.	Department of Geology, Central University of Venezuela
Executive Committee	
Name	**Affiliation**
Nasir Ahmadi	Environmental Protection Organization of Mazandaran Province
Arash Amini	Golestan University
Alireza Amrikazemi	Scientific Coordinator, Qeshm Island UNESCO Global Geopark
Parviz Armani	Imam Khomeini International University
Ataollah Dadashpour	Geological Survey of Iran, Sari branch
Asghar Dolati	Kharazmi University
Hasan Fazelinashli	University of Tehran
Fahimeh Foroghi	Iranian National Institute for Oceanography and Atmospheric Science
Abdolazaim Ghanghormeh	Golestan University
Habibolah Ghasemi	Shahrood University of Technology
Mohammad reza Ghasemi	Research Institute for Earth Sciences
Manouchehr Ghorashi	Research Institute for Earth Sciences

Jafar Hassanpour	University of Tehran
Ataollah Kavian	Environmental Protection Organization of Mazandaran Province
Mohammadreza Kazemzadeh	Superme Audit Gourt
Razyeh Lak	Head of RIES and Executive Manager
Majid Moghadam	Iranian Research Organization for Science & Technology (IROST)
Mahmoudreza Majidifard	Research Institute for Earth Sciences
Ali Akbar Momeni	Shahrood University of Technology
Babak Moradi	Iranian National Institute for Oceanography and Atmospheric Science
Seyed Mohsen Mortazavi	Hormozgan University
Hasan Nasrollah Zadeh Saravi	Caspian Sea Ecological Research Center
Ehsan Pegah	Kharazmi University
Abdolwahed Pehpouri	Qeshm Island UNESCO Global Geopark
Ahmadreza Rabani	University of Science and Technology of Mazandaran
Mahdi Rahmanian	Shargh Daily newspaper
Ahmad Rashidi	International Institute of Earthquake Engineering and Seismology
Masoud Sadri Nasab	University of Tehran
Mohammad Salamati	Respina Company

Mohammad Tatar	International Institute of Earthquake Engineering and Seismology
Alireza Vaezi	Research Institute for Earth Sciences
Mojtaba Yamani	University of Tehran
Ahmed Hadidi	German University of Technology in Oman (GUTECH)
Secretariat	
Name	**Affiliation**
Elnaz Aghaali	Research Institute for Earth Sciences
Keivan Ajdari	Research Institute for Earth Sciences
Hourieh AliBeygi	Research Institute for Earth Sciences
Sedigheh Ghanipour	Research Institute for Earth Sciences
Hamoon Memarian	Research Institute for Earth Sciences
Shirin Safavi	Research Institute for Earth Sciences
Aazam Takhtchin	Research Institute for Earth Sciences
Mehrnoosh Pour Saeid	Graphic Designer
Hanieh Bakhshaei	Geological Survey of Iran
Reza Behbahani	Geological Survey of Iran
Javad Darvishi khatooni	Geological Survey of Iran
Mohammadreza Ensani	Geological Survey of Iran
Marziyeh Estrabi Ashtiyani	Geological Survey of Iran
Gholamreza Hoseinyar	Geological Survey of Iran
Mojtaba Kavianpour Sangno	Geological Survey of Iran

Contents

Table of Figures

Table of Table

ABSTRACT

The evaluation of seismic potential of the Astara fault, with a length of about 110 km and considering the residence of more than 150.000 people within the fault zone, is of great importance. The Astara fault with a general N-S trend, is located on the eastern border of Talesh Mountains. Hitherto, the largest earthquake (Mw 6.6) in this vicinity has been recorded at a distance of 15km from the Astara fault.

Geometrically, the Astara fault as an active fault zone, kinematically could be distinguished as a wide zone consists of two major faults: (1) Astara thrust fault (ATF) which is located close to the mountain range. (2) Active Astara strike-slip fault (ASF).

Measured maximum and minimum horizontal displacements along the fault are 1500 m and 70 m respectively, and maximum and minimum vertical displacements are 130 m and 5 m respectively. Present estimated rake value is 0 to 12 towards SW with a slip rate ~ 1.5 mm/yr. On the basis of Paleoseismological investigations in Lisar Trench, and using C^{14} age determinations, it is evident that at least 3 to 4 Paleoearthquakes with magnitudes Mw 6.24-5.74 occurred around 30.000 year ago, and based on the sedimentation rated of trench layers, the estimated magnitude of the youngest (~ 5.000 yrs.) and oldest (~30.000 yrs.) events are Mw 6.24 and Mw 5.74 respectively.

Chapter One

GENERALITIES AND BASIC CONCEPTS

1-1- Introduction

Today, more than two million people live in territory of the Astara fault. Therefore, in order to avoid human and financial damages due to earthquakes in this area, tectonic and seismological researches are considered inevitable. This is while the statistical comparison of instrumental earthquakes from the last century until now, along with the historical earthquakes reported in this area, have revealed the tectonic activity for this region. Therefore, the value of knowing more about the geodynamic processes of this structural zone increases. With this regard, one of the useful approaches to obtain the long-term seismic history of an active fault is paleoseismology. Paleoseismology, is a link between the knowledge of seismology and geology, and deals with the geological investigation of earthquakes that occurred decades, centuries, and thousands of years ago.

In this study, an attempt has been made to reveal the seismic history of the Astara fault system by applying the morpho-tectonics and paleoseismology investigations in the south Caspian basin.

1-2- Upcoming questions

Since the instrumental and historical seismic data cover a small part of the seismic history of a fault, in order to obtain the background seismicity of a fault and identify how it functioned in the past, it is necessary to conduct paleoseismological researches. In this purpose, paleoseismological researches have been conducted along the Astara fault, and the main aim of this study is to complete the existing seismic data and to obtain the seismic history of this fault in longer periods. There are certainly many questions that cannot be answered by only available instrumental and historical data. The main questions of this study are as follow:

- Does the past mechanism of the Astara fault continue today or has it changed?
- What was the magnitude of paleoearthquakes?
- Do the paleoearthquakes on the Astara fault follow a clear seismic pattern?
- What was the return period of paleoearthquakes?
- Is it possible to provide a long-term prediction of the next large earthquake event?

1-3- Procedure of investigation

In paleoseismological research, the first and most fundamental step is to determine the location of the trench on the fault. For this purpose, using ASTER satellite images with a spatial resolution of 30 meters, IRS with a spatial resolution of 5.8 meters, as well as examining the geomorphological and seismological maps of the Talesh ranges (Kaveh Firouz et al. 2013), an executable location for trenching was selected along the Astara fault.

The sedimentary units in the trench wall were mapped with an accuracy of 1:20, and the magnitude of each event was estimated by using the existing relationship (Wells and Coppersmith. 1994).

1-4- General characteristics of the region

1-4-1- Geography of the studied area

Gilan province in north of Iran, has an international border with the Republic of Azerbaijan (through Astara), and limited to, Ardabil province from the west, Zanjan and Qazvin provinces from the south, and Mazandaran province from the east. The paleo-seismological site of the Astara fault is located at latitude 37.96830 and longitude 48.89810, located in Lisar village (Figure 1).

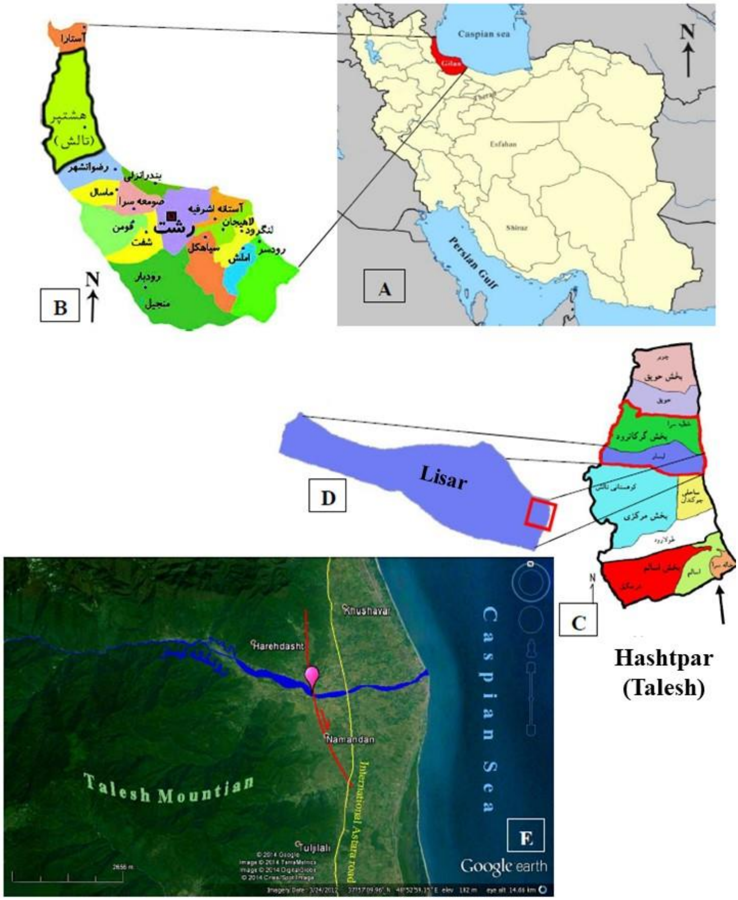

Figure 1: Geographical location of the selected paleoseismological site on the Astara fault. (A) The province in red is Gilan province. (B) The map of the cities of Gilan province. The city that has a sharper border is the city of Talesh, where paleoseismological studies have been carried out. (C) The map of Talesh (Hashtpar) city districts, and Lisar village location. (D) Lisar district, the red square shows the location of the Google Earth satellite image. (E) Google

Earth image of the studied area, the pink balloon shows the location of the Lisar paleo-seismological trench.

1-5- Tectonic and geological setting of the Astara fault system

Iran is located in the middle of Alpine-Himalayan folded belt, in a compressive zone arising from the convergence of the Arabian and Eurasian plates. The convergence caused deformation of the regional continental crust, with an area of approximately 3,000,000 square kilometers, which is the largest deformed region in the world (Allen, 2004). The convergence of Arabian-Eurasian plates with a rate of more than 22 mm/y caused a complex system of reverse and strike-slip faults. This has also been phenomenon confirmed quantitatively using GPS data (Vernant et al. 2004). It is worth noting that strike-slip faults have the potential to produce large earthquakes (Kurushin et al. 1997; Berberian et al. 2000; England & Molnar, 1990). Most continental strike-slip fault zones are located in quasi-shear environments (compared to pure shear environments) resulting from oblique convergence or divergence at plate boundaries.

In north-west of Iran, the existence of shear movements has caused the creation of strike-slip faults, of which the Astara fault system is one of the prominent examples. Gilan, as one of the most populated provinces, with a population of more than 2 million people, is located in this active strike-slip zone. The 1709 and 1713, historical earthquakes which caused the destruction of the Rasht area in the 18th century, can be considered as the result of movement of the southern part of this fault system.

The Astara fault system, with a north-south trend in the northern part and a northwest-southeast direction in the southern segment, in the form of a 110 km long right-lateral compressional system, forms the eastern border of Talesh renges with respect to the Caspian Coastal Plain (Figure 2; Nazari et al., 2014).

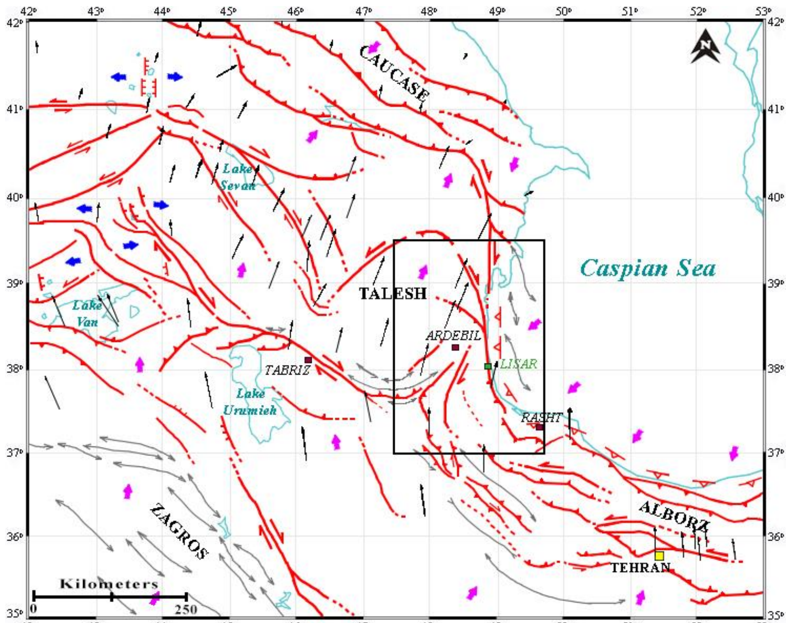

Figure 2: Interpretive geodynamic map of northwestern Iran. The purple arrows show the direction of compression and the blue

arrows show the direction of extension. The black arrows indicate the GPS vectors and the bidirectional gray arrows are fold axis. As can be seen, in the figure, in the vicinity of Astara fault (inside the black square), the direction of the GPS vectors is angular to the direction of the Astara fault, which justifies the right-lateral movement of the fault. The city of Lisar, (green colore), shows the location of the paleoseismological trench. The black square indicates the location of Figure 5-1 (adapted from Reilinger et al. 2006).

In order to show more clearly the tectonic setting of the Astara fault, combination of the MrSid satellite image, with the SRTM satellite data (with a spatial resolution of 90 meters), has been used (Figure 3).

The strike-slip mechanism of the Astara fault, especially in the northern and middle parts, with north-south trend, and shutter ridge features can be seen along the Talesh ranges (Nazari et al., 2014).

In order show more clearly the location selected for paleoseismological research along the Astara fault, the IRS satellite image with spatial resolution of 5.8 meters was used (Figure 5). On this image, the righ-lateral displacement of the Lisar River by the Astara fault can be clearly seen.

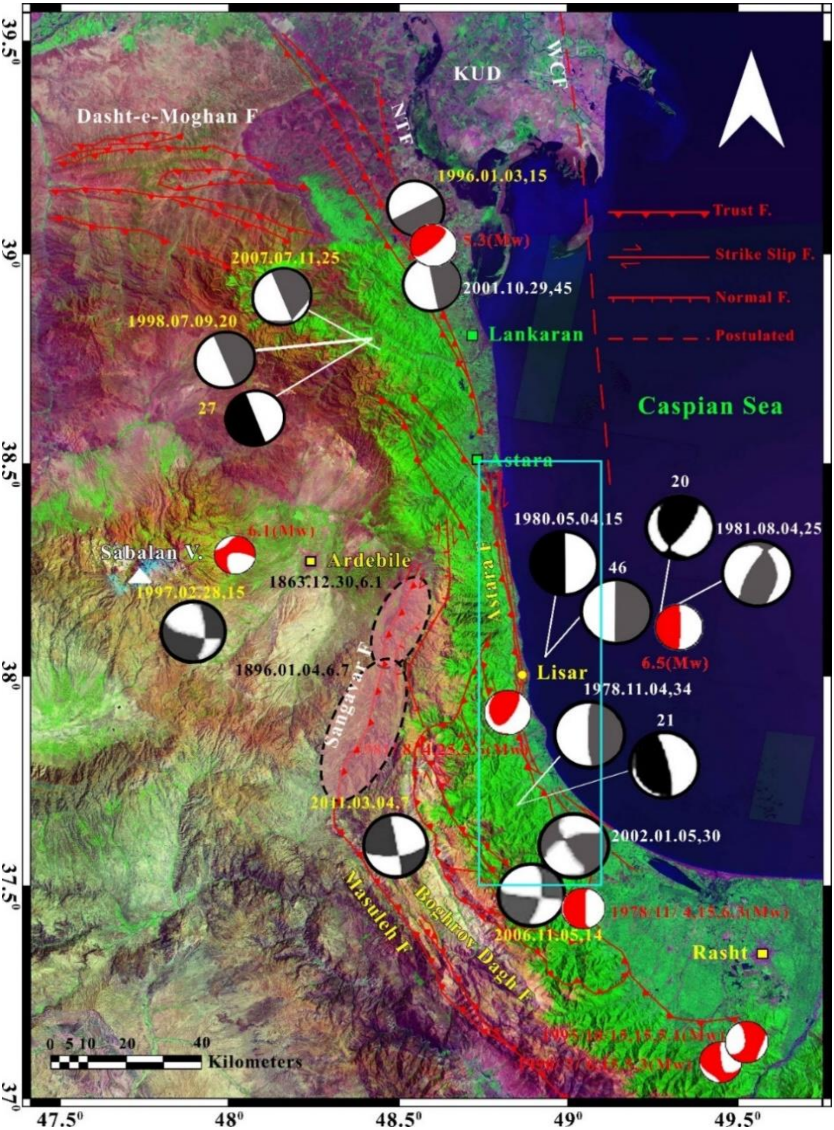
KUD
WCF
NTF
Dasht-e-Moghan F
1996.01.03,15
5.3(Mw)
2001.10.29,45
2007.07.11,25
1998.07.09,20
27
Trust F.
Strike Slip F.
Normal F.
Postulated
Lankaran
Caspian Sea
Astara
20
1980.05.04,15
1981.08.04,25
46
6.5(Mw)
Sabalan V.
6.1(Mw)
Ardebile
1863.12.30,6.1
1997.02.28,15
1896.01.04,6.7
Lisar
1978.11.04,34
21
Sangavar F
2011.03.04,7
2002.01.05,30
2006.11.05,14
Masuleh F
Boghrov Dagh F
Rasht
0 5 10 20 40
Kilometers
39.5°
39°
38.5°
38°
37.5°
37°
47.5°
48°
48.5°
49°
49.5°

Figure 3: Seismotectonic map of Talesh Heights, which is prepared by combining MrSID satellite image with Digital Elevation Model (DEM) obtained from SRTM data (with spatial resolution of 90 meters). The epicenter and mechanism of earthquakes in the period of 04/11/1978 to 04/03/2011 are shown. 4 events with black focal mechanism were determined by Jackson et al. (2002); The 10 gray events are related to the central-moment-tensor focal mechanism solution (http://www.globalcmt.org/CMTsearch.html). The focal mechanism located on the Masule fault, related to the moment tensor solution of the March 4, 2011 event (ML=4.2) from Aziz Zanjani et al. 2013; Mechanisms in red are taken from the global focal mechanism solution of CMT. The dashed blue square shows the location of Figure 4.

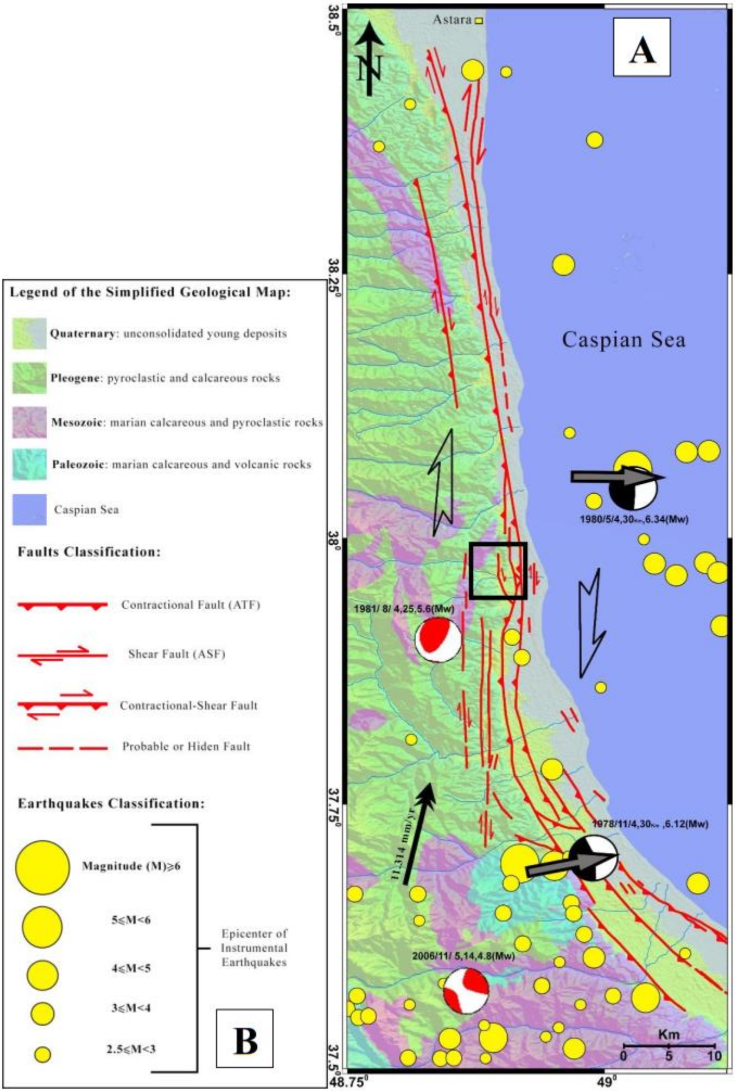

Figure 4: Simplified geological map of Talesh ranges and Astara fault system, yellow circles show the instrumental earthquake

epicenters. The dark arrow, indicating the GPS velocity vector, and the pink arrow, show the dominant mechanism movement of the Astara fault. The black rectangle, is location of figure 1-7.

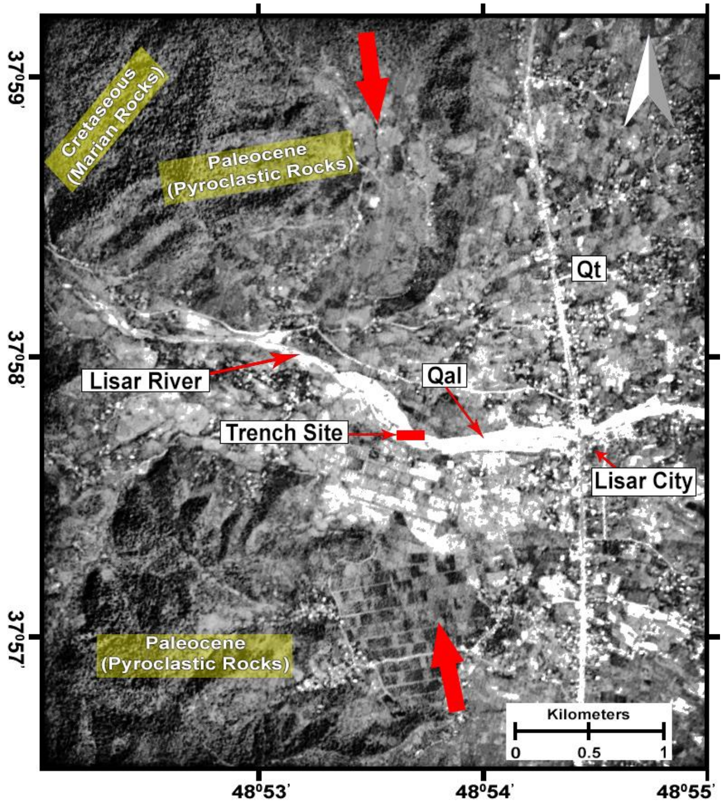

Figure 5: IRS satellite image with spatial resolution of 5.8 meters, from the area selected for paleoseismological trenching. The red square shows the location of the paleoseismological trench and the red arrows show the trace of the Astara fault.

Chapter two

SEISMOTECTONICS AND MORPHOTECTONICS CHARACTERISTICS OF THE STUDY AREA

2-1- Seismotectonics of the study area

The South Caspian Basin (SCB), on the southern edge of the Eurasian Plate, is a rigid shield block that has been very effective in the deformation and seismology of its surrounding regions such as the Caucasus, Talesh, Alborz, and Kopeh Dagh mountain ranges (Berberian 1983; Jackson & McKenzie 1984; Jackson et al. 2002) (Figure 6). Previously, the South Caspian Basin was considered a rigid block due to the lack of significant intrabasin seismicity (Ambraseys & Melville 1982; Berberian 1983; Jackson & McKenzie 1984; Priestley et al. 1994; Jackson et al. 2002). Along the southwestern coastline of the Caspian Sea, most of the seismic data are obtained from regional networks and remote seismographs or historical and instrumentally recorded earthquakes.

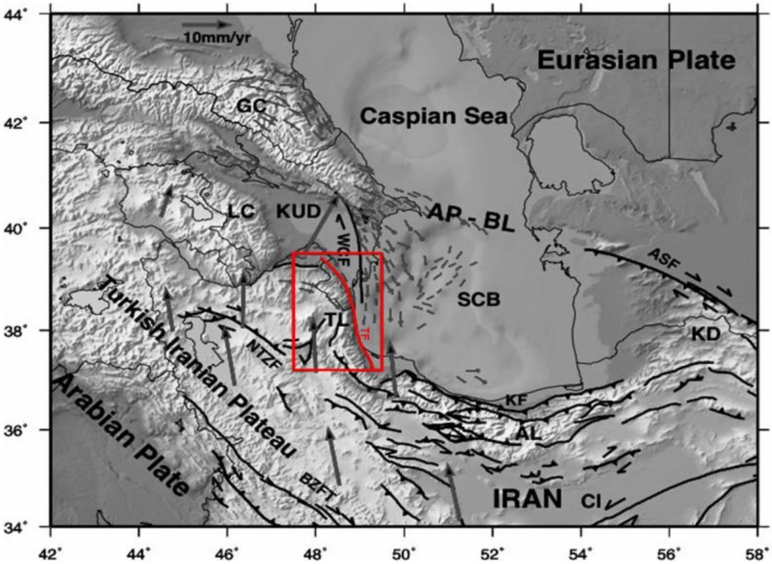

Figure 6: Relief map of South Caspian, Talesh and its surrounding areas. Faults and fold axis are shown by black and gray lines, respectively. The red square shows the position of Figure 2-2 and 2-3. Abbreviations: South Caspian Basin (SCB), Central Iran (Cl), Talesh ranges (TL), Great Caucasus (GC), Little Caucasus (LC), Alborz montains (AL), Kopeh Dagh (KD), Kura Depression (KUD), West Caspian Fault (WCF), Talesh Fault (TF), North Tabriz Fault (NTZF), Caspian Fault (KF), Ashgabat Fault (ASF), Apsheron-Balkan Siff (AP-BL). Faults from Hessami et al. (2003) and Jackson et al. (2002). GPS vectors from Djamour et al., (2011); Aziz Zanjani et al., (2013).

Jackson et al. (2002), determined focal mechanism solutions for four events with a focal depth of 15-27 km along the western shore of the Caspian (Figure 7), which indicated faulting in the basement of the South Caspian basin. The focal mechanism of the earthquakes in the western margin of the South Caspian basin, indicating northward trend, shallow-depth low angle thrust dipping toward the west, where coincide with the thrust under the basement of south Caspian basin. Although no fault reported with the same trend of south Talesh, but there are some evidences for a right-lateral strike-slip fault west of the Kura depression and Talesh mountain (Priestley et al. 1994; Berberian & Yeats 1999; Jackson et al. 2002). Talesh and Caspian faults have been identified as the most important structures responsible for devastating earthquakes in the last 1100 years in the western and southern parts of the South Caspian basin, respectively (Berberian 1983).

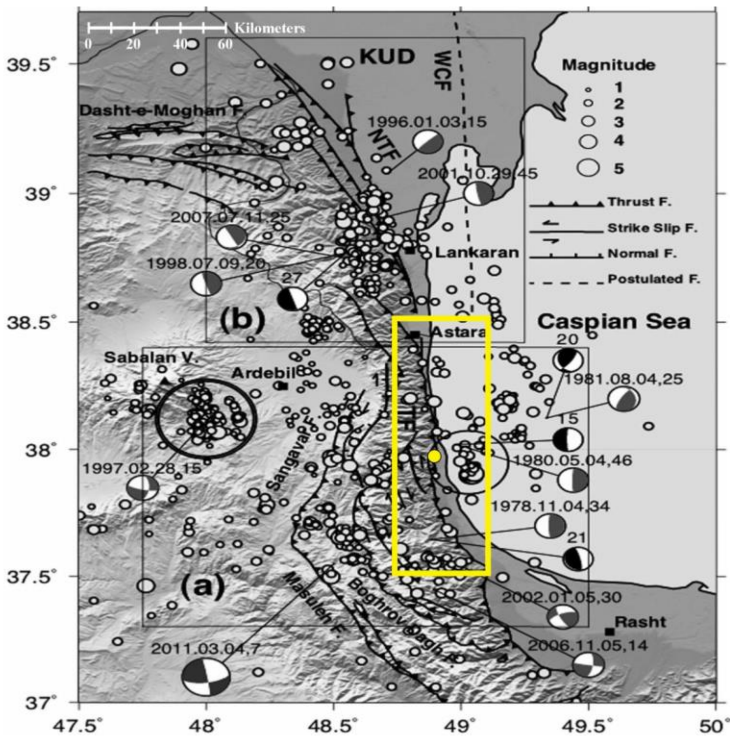

Figure 7: Seismotectonic map of Talesh Heights. Events from October 11, 2009 to December 30, 2011 were recorded by the IASBS local network. The thick black circle in the southeast of Sablan volcano shows a series of events related to the Golestan-Ardebil earthquakes (February 28, 1997, MW = 6.1). The thin black circle shows a group of events related to the Hashtpar-Gilan earthquakes and its aftershocks (October 22, 2010, ML = 5). The focal solution of the earthquakes in gray are part of the global CMT solution for 10 events in this region. Near each, the time and depth of the event are indicated. Mechanism and focal depth of 4 events in black estimated by Jackson et al. (2002). The focal solution with the great circle on the Masouleh fault is the moment tensor solution for the 4 March 2011 event (ML = 4.2). Quadrants a and b are the southern and northern seismic bands. The red square shows the

study area, and the red circle shows the location of the Lisar paleoseismological trench (Aziz Zanjani et al. 2013).

According to Aziz Zanjani et al. (2013), western coast of the Caspian basin and the Talesh montain is undergoing active faulting (Figure 8 & Figure 9). While seismicity is located in the eastern part of the Talesh thrust fault with a dip towards the west, so it cannot be related to this fault. Even, there is no strong evidence that this seismicity structurally is related to the trend of the right-lateral West Caspian Fault (WCF) identified in the region. A dextral fault has been identified in the northern part of Talesh, located in the southwest of the Kura basin, but its extension to the south and inside the South Caspian basin is unknown. Aziz Zanjani et al. (2013) also calibrated a significant number of focal depths in the depth range of 59 to 74 km from the southernmost parts of Talesh towards the southern border of the Kura basin. The obtained depths also confirm the subduction of the South Caspian basin.

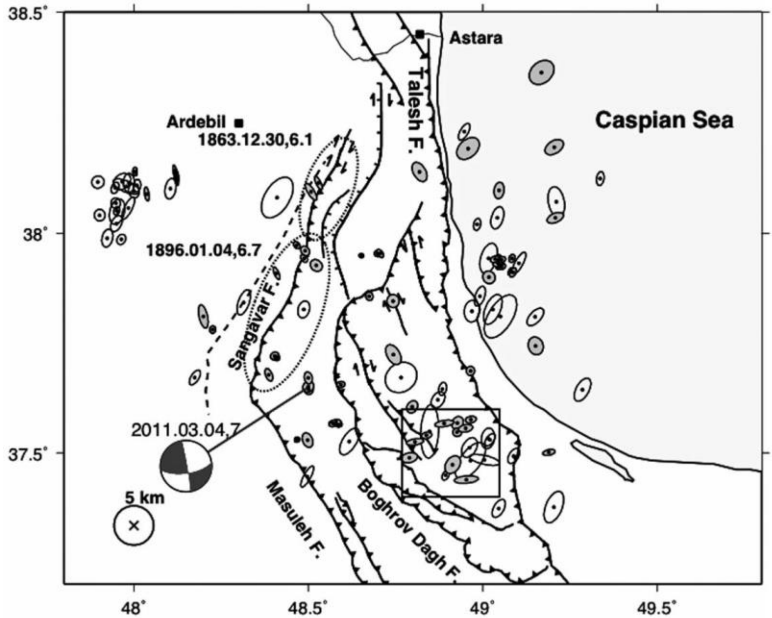

Figure 8: The epicenters of the earthquakes in the southern cluster that have been re-located based on the HDC-method. Each location is shown with a 90% confidence ellipse. White ellipses are for EBH catalog events and gray ellipses are for events recorded by the IASBS network. The focal mechanism for the March 4, 2011 earthquake obtained by Aziz Zanjani et al. (2013). A circle with a radius of 5 km is shown as a measure of error. The two large dotted ellipses show the macroseismic region of the two large earthquakes of 1896 and 1863 (Berberian & Yeats 1999). The black square indicates the orientation of events that are not consistent with known faults (Aziz Zanjani et al., 2013).

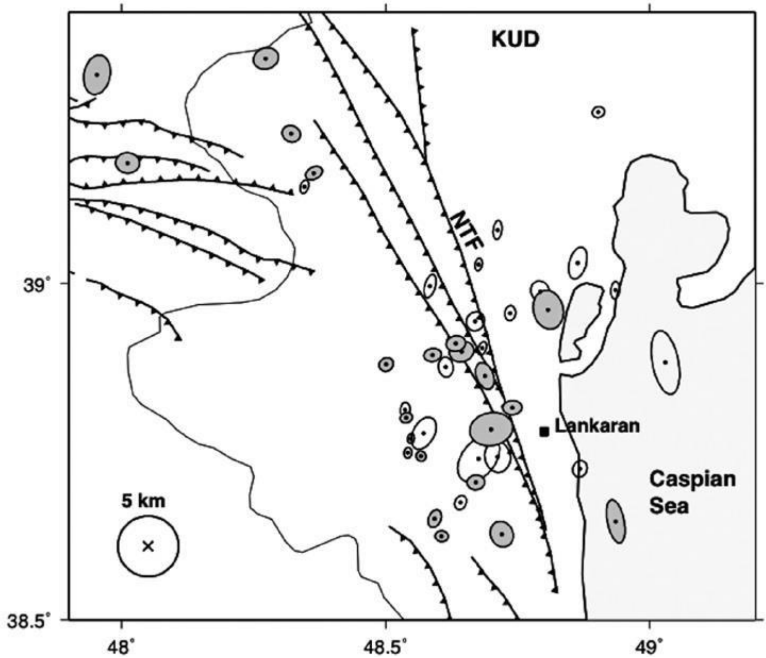

Figure 9: The earthquakes epicenters of the northern cluster that have been re-located based on the HDC-method. The thin black line shows the Iran-Azerbaijan border. The NTF is the North Talesh fault (Aziz Zanjani et al. 2013).

Figure 10 shows the depth distribution of events with focal depth of more than 20 km. This is a deformation corresponding to the faulting of the South Caspian basement under the Talesh and Kura down-thrown. With regards to the surface distribution of the earthquakes, it can be said that the Caspian basement thrusted nearly 20 to 25 km underneath the Talesh.

Triangles are events with a known focal mechanism. These events with at a depth of 27 to 32 km, are corresponds to the fault near the basement surface or beneath the sedimentary cover. The large depth range (20 to 45 km) of the events inside the South Caspian basin indicates that the Caspian crust is very stable, rigid and resistant. Mangino and Priestley (1998) believe that the basement of the Caspian will be thicker towards the western shores. The observed depth of seismicity also confirms the thickness of the crust under the Caspian basin. A similar pattern can be seen in the south of Talesh (Figure 10b). Deep earthquakes (18 to 34 km) occur in the Caspian basement. As can be seen in Figure 10, the main branch of the earthquakes in coastal zone is consistent with the structural bending of the north and south of the segment Talesh Heights and indicates a severe deformation in these areas. In the north of Talesh, the seismicity is more in the eastern part than in the west, which indicates that the deformation is currently concentrated in the eastern side, and as it is evident from the depth of the seismicity, the oceanic crust of the Kura trough is subducting under the Talesh.

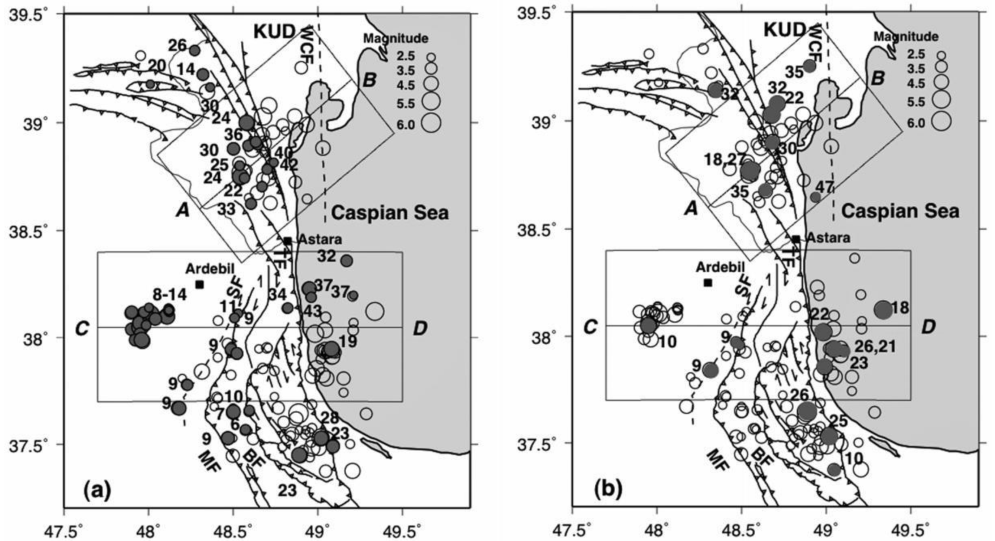

Figure 10: Depth distribution of earthquakes in Talesh ranges. Epicenters of earthquakes based on HDC-relocation in two clusters are shown by circles with sizes consistent with local magnitude. (a), earthquakes whose depths have been calibrated using local phases are shown with solid circles. (b), the earthquakes whose depths have been calibrated using teleseismic phases are shown with solid circles and the obtained depth shown next to the event (Aziz Zanjani et al. 2013).

All the earthquakes with less focal depth are located in the western side of Talesh ranges and are indication of deformation of the upper continental crust in this region. It seems that the under thrusting of the Caspian basement under the central part of Talesh is less than to its north. In Talesh, seismicity is concentrated in its northern and southern structural arcs, with less seismicity in central part. Shallow earthquakes are not seen on the eastern edge of the entire length of the ranges. According to Aziz Zanjani et al. (2013) the basement of the South Caspian basin is the main cause of seismicity in the region. The depth of the seismicity reaches to 47 km, which is an indicator of the subduction of the South Caspian basement beneath Talesh. The depth of seismicity is obviously lower than the subduction of the northern border of the basin in Apsheron region (depth of 80 km). In the central and southern Talesh, the rate of subduction is lower than in the northern part. Therefore, it seems that under thrusting might be in the first stages of formation (Figure 11). Despite strong evidence of dextral strike-slip motion in Talesh, there is no alignment in seismicity to delineate a single north-south structure. However, as Jackson et al. (2002), suggested, right-rotating shear deformation may be distributed over the sedimentary cover rather than acting on a single fault. It seems that these dextral movements are compensated on a set of known and unknown faults in the south of Talesh.

Kaveh Firouz et al. (2013), believe that due to the geometry of the South Caspian Basin characteristics the possibility of a large earthquake along the Astara fault system or a tsunami event in the western and south-western parts of the Caspian coast, it will not be far from the expectation.

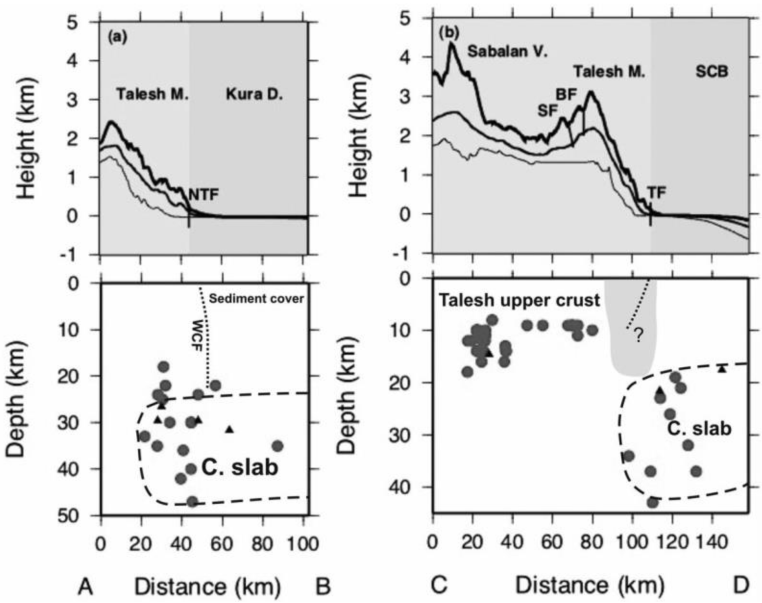

Figure 11: Deep profiles together with the topographical changes along AB and CD lines specified in Figure 10. (a) for the northern cluster and (b) for the southern cluster. Triangles are events with focal mechanism (from the CMT catalog) (Figure 10). The dashed line shows the Caspian basement based on seismic data. WCF location based on profile interpreted from Allen et al. (2003), that they considered this fault to be the boundary between the sedimentary cover and the Talesh continental crust. The shaded

region in (b) is the aseismic region below the central Talesh. TF is Talesh fault, SF is Sangavar fault and BF is Boghro-Dagh fault (Aziz Zanjani et al. 2013).

Although it is not possible to estimate the recent activity rate of the Astara fault system based on only one GPS station on one side of the fault, but based on the data obtained from other stations of the geodynamic network in the southern coasts of the Caspian and also west of Talesh ranges and geological features such as 15 km thickness of Neogene deposits in the South Caspian basin, the maximum rate of young movement of the Astara fault is considered up to 1.5 mm/yr (Figure 12; Nazari et al. 2013).

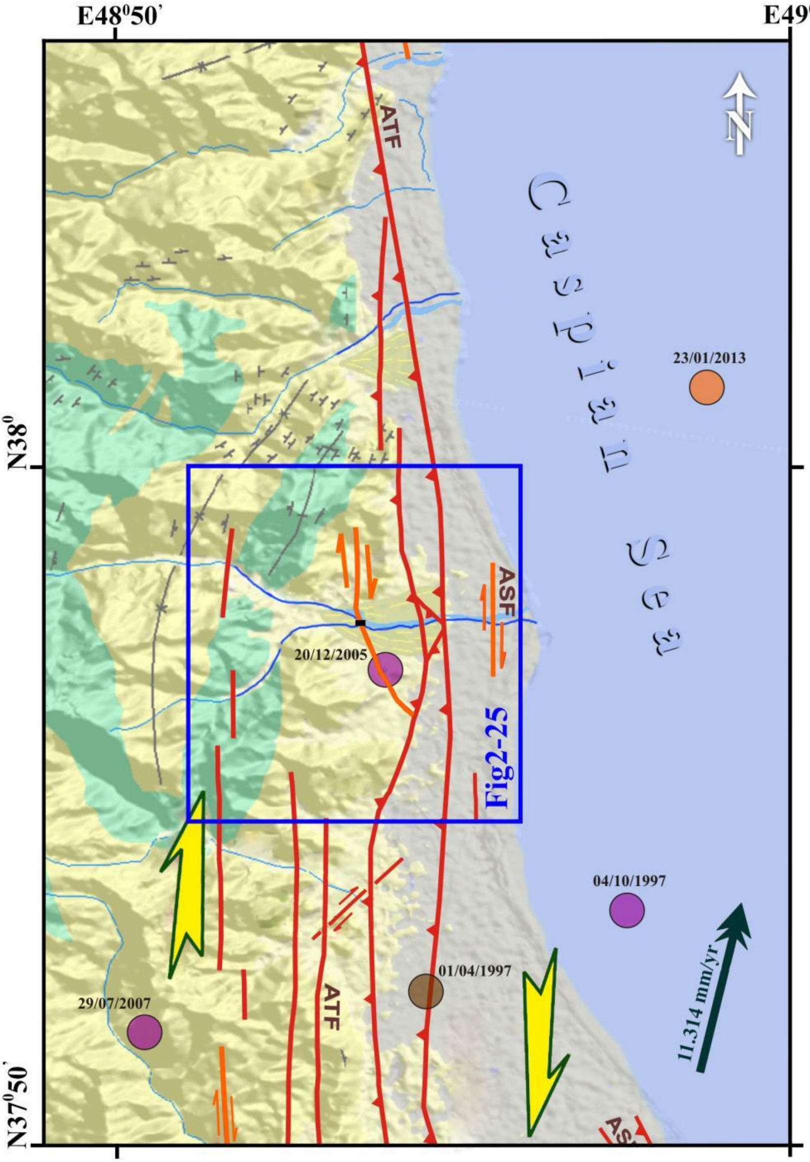
E48°50'
E49°
N38°
N37°50'
N
ATF
Caspian Sea
23/01/2013
ASF
Fig2-25
20/12/2005
04/10/1997
01/04/1997
29/07/2007
ATF
11.314 mm/yr
AS

Figure 12: A part of the seismotectonic map of the Astara fault (Kaveh Firouz et al., 2013). The colored circles show the epicenter of the instrumental earthquakes.

In spite of the lack of radiometric dating data from young sediments affected by the Astara fault, it can be assumed that the estimated slip rate of 1.5 mm/y for the Astara fault is in accordant with the historical and instrumental earthquakes. The location of paleoseismological trenching is shown in Figure 13.

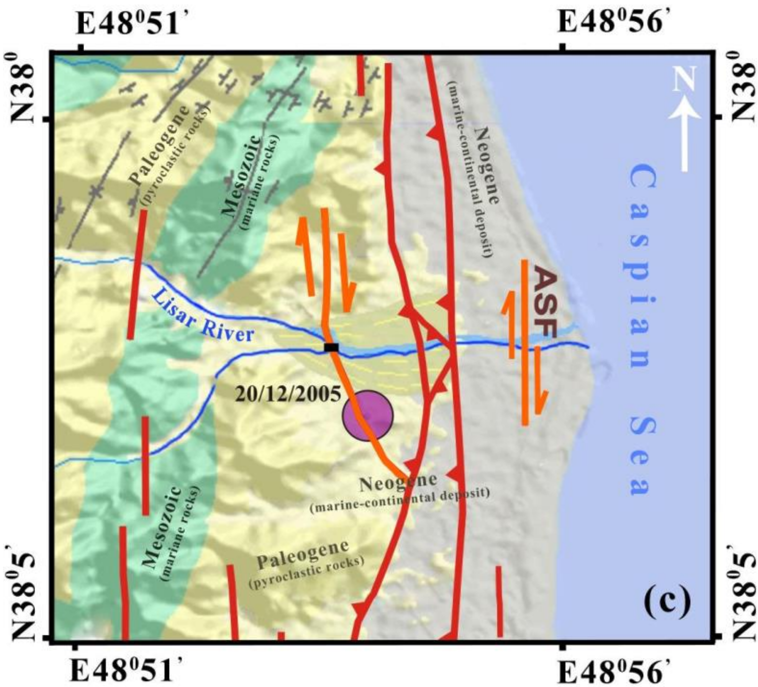

Figure 13: A close-up view of the ASF branch of the Astara fault, on which paleo-seismological researches have been conducted. The black square shows the location of the paleoseismological trench.

2-2- Morphotectonic characteristics of the study area

The Talesh mountain ranges are located with a north-south trend in northern Iran, west of the Southern Caspian Sea Basin, in the continuation of the Alborz Mountains. The Astara fault, with a length of about 110 km and a dip towards the west, constitutes the eastern part of the Talesh mountain range. The bending of the fault towards the southeast in the southern parts shows that the compressional component of this part is dominant compared to the northern parts. Based on morphotectonic studies, one of the main reasons for the shortening of Talesh towards the east can be related to the activity of the Astara fault zone.

Based on geomorphological and seismotectonic studies by Kaveh Firouz et al. (2013), the Astara fault, consists of 2 segments: 1- Astara thrust fault (ATF) which is located in the mountain front and has 3 parts and thrusted Cretaceous and Paleogene units on Quaternary alluvial deposits. 2- The Astara strike Slip Fault (ASF), which is located in the western part of the South Caspian coastal plain.

The maximum and minimum horizontal displacements (H) on the Astara thrust (ATF) in segment-1 is estimated to be 1500 and 190 meters respectively, and the maximum and minimum vertical displacement (V) of this branch of the Astara fault system is 130 and 10 meters respectively, which indicates the maximum H/V ratio of 13 for the ATF fault of the Astara fault system. Right-lateral strike-slip mechanism of the Astara fault, especially in the northern and middle parts, where the dominant trend of the fault is N-S, more morphological indices, such as shutter ridge, river offset, etc. can be seen, The maximum measured displacement along the ATF1 system was estimated to be nearly 840 meters, and the minimum displacement was estimated to be approximately 90 meters for ATF3, and nearly 70 meters for ASF2. The maximum vertical displacement was measured around 130 meters for ATF2 and the minimum at around 5 and 10 meters for ASF, ATF.

The fault segment studied in this study is located in segment-1 of the ASF fault branch, with the strike-slip mechanism. Based on Table 1, it can be seen that each morphotectonic segment of the fault system has minimum and maximum rake. In this regard, for the magnitude calculations of the historical earthquakes identified in the Lisar trench, the mean rake segments of the ASF fault branch have been used.

Table 1: The result of the morphotectonic and seismotectonic studies along the Astara fault (Kaveh Firouz et al. 2013).

ASTARA ACTIVE FAULT SYSTEM													
Fault name	Segment	Length (km)	Azimute	Dip	Mechanism	H (m)		V (m)		Rake/ segment	Slip Rate (mm/yr)	Earthquake Related	
						H min	H max	V min	V max			Instrument	Historical
Astara Thrust Fault (ATF)	1	≤13	346°	70° - 80°	Strike slip (right lateral), Thrust	190	1500	10	15	0.3° - 4°	~ 1.5	**24-06-1903;** mb=5.5 (AMB) **24-06-1907;** ms=5.9 (AMB) **11-07-1970;** mb=5.2 (EHB) **4-11-1978;** mw=6.3 (EHB) **4-05-1980;** mw=6.5 (EHB) **5-11-2006;** mn=5 (ISC) **23-03-2008;** mn=5 (ISC)	1709 AD ?? 1713 AD ??
	2	≤63	354°	80° - 90°	Strike slip (right lateral), Thrust	90	1000	10	130	5.7° - 7.2°			
	3	≤32	322°	60° - 70°	Thrust, Strike slip (right lateral)	90	900	10	95	6.3° - 11.9°			
Astara Strike slip Fault (ASF)	1	≤40	356°	80° - 90°	Strike slip (right lateral)	80	840	5	30	1.9° - 6.8°			
	2	≤24	316°	60° - 70°	Thrust, Strike slip (right lateral)	70	500	5	40	0.6° - 4°			

Chapter three

PALAEOSEISMOLOGICAL INVESTIGATION ALONG THE ASTARA FAULT

3-1- Introduction

Following seismotectonic and morphotectonic investigations by Nazari et al. (2013) and Kaveh Firouz et al. (2013) in west Caspian region, paleoseismological studies carried out along the Astara fault.

3-2- Design and selection of the paleoseismological trench site along the Astara fault

The existence of instrumental seismic data (including macroseismic and microseismic) and historical data indicates seismic potential of the area (for example, Tsukuda, 1985; Wallace, 1978, 1981). Morphological and seismological evidences clearly indicate the movement of the Astara fault in the Quaternary period (Nazari et al. 2013; Kaveh Firouz et al. 2013; Aziz Zanjani et al. 2013). Therefore; after carrying out office checks on ASTER satellite images (with a spatial resolution of 30 meters), IRS (with a spatial resolution of 5.8 meters), three-dimensional topographic data of SRTM (with a spatial resolution of 30 meters), geomorphological and seismotectonic maps of the Talesh ranges together with geological maps of

Astara and Khalkhal-Rezvan Shahr (both on a scale of 1:100,000) and existing dissertations, reports and articles on the Astara fault, a comprehensive field visit carried out in order to select the appropriate location, for paleoseismological studies.

The Lisar trench is 1.3 km away from the center of Lisar city, and because the Lisar trench itself was a natural trench, it played an important role in choosing this site for paleoseismological research.

The length of the Lisar trench is about 12 meters, is almost perpendicular to the general direction of this segment of the Astara fault (N170). In this study, a paleoseismological log of 11.5 meters was prepared from the wall of the Lisar trench with a scale of 1:20.

The main reasons for choosing this trench are as follows:

- Cut off of the alluvial deposits of the Lisar river wall by the fault (Figure 14);
- Geomorphological evidence indicating the right-lateral movement of the Lisar River by the Astara fault;
- Easy access to the fault zone for excavation and subsequent field observations;

In Figure 14, the panoramic view of the Astara fault zone in the wall of Lisar trench and in Figure 15 its sedimentary texture and paleo-seismological log are shown.

The description of segregated sedimentary deposits in the fault zone is given in Table 2. In Figure 16 the occurrence horizons of paleoearthquakes and in Table 3 the evidence of these horizons; and finally, in Figure 17, the paleoseismological log that is currently surveyed are shown.

As mentioned earlier clay units were sampled for carbon 14 dating method. The locations of the collected samples in the paleo-seismological log are shown with red circles under the names C_1 to C_6. According to Nazari (Oral communication, 2014), the age of the alluvial deposits on the left side of the trench wall (Unit 3) is estimated to be 30 ka, and the age of the mud deposits on the right side (Unit 11) is estimated to be 12 ka".

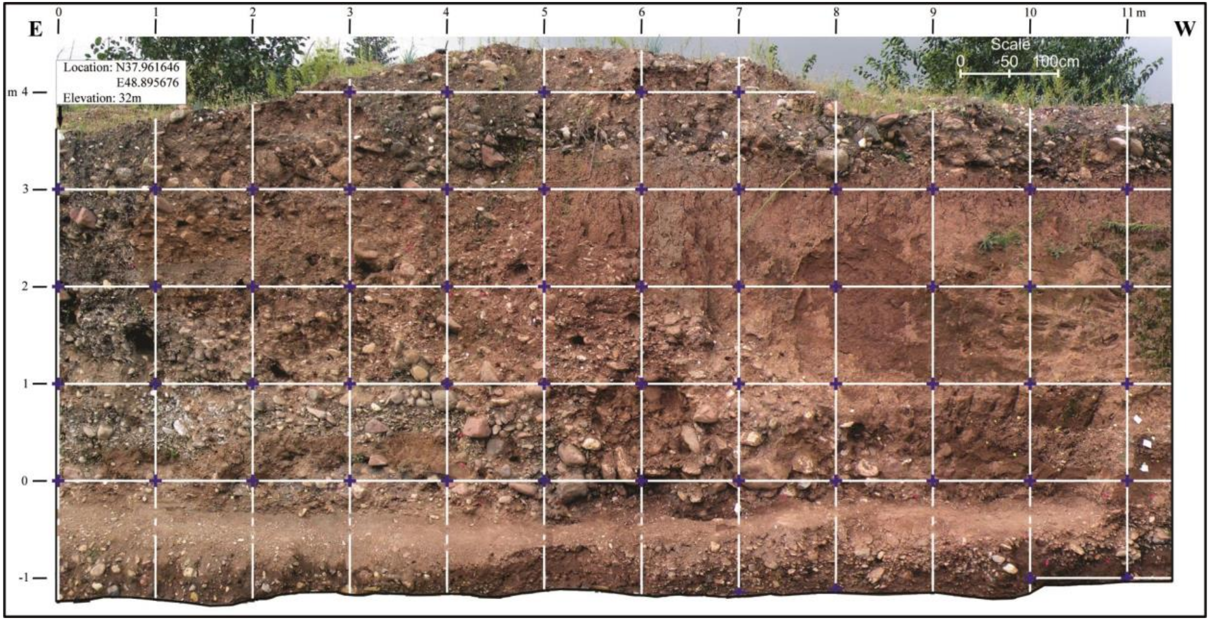

Figure 14: General view of the main fault zone on the right wall of the Lisar river.

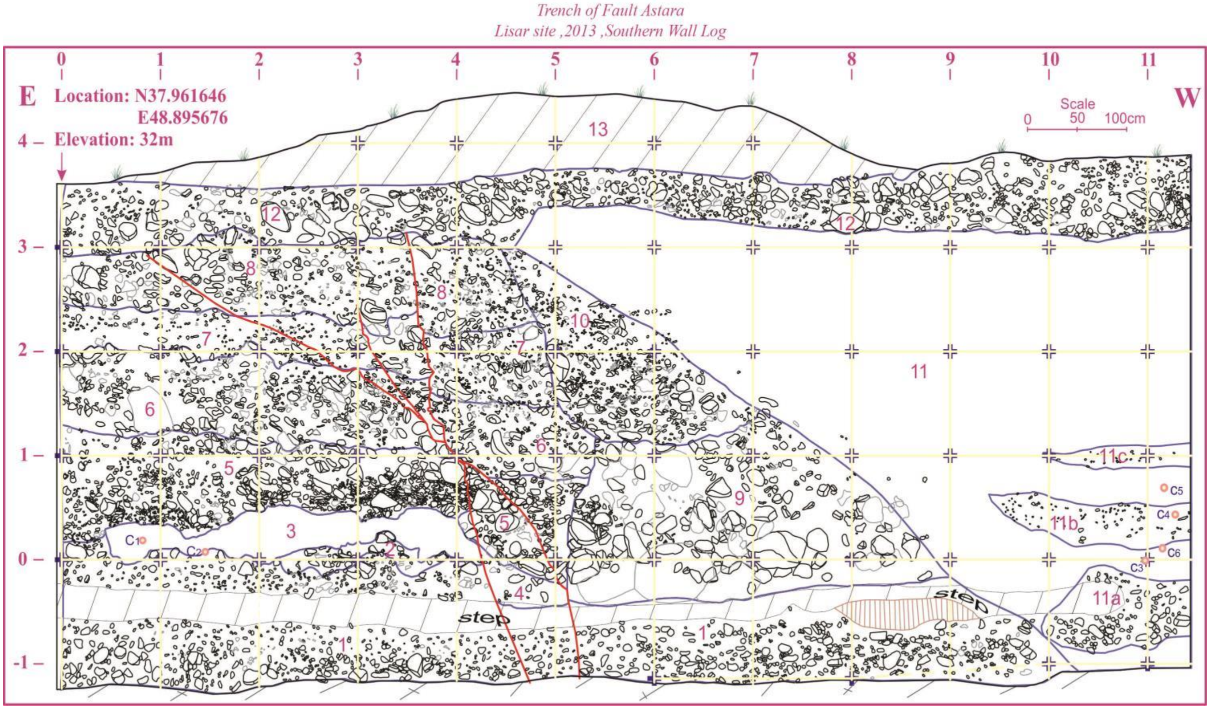
Trench of Fault Astara
Lisar site ,2013 ,Southern Wall Log
E
W
Location: N37.961646
E48.895676
Elevation: 32m
Scale
0
50
100cm
0
1
2
3
4
5
6
7
8
9
10
11
4
3
2
1
0
-1
13
12
12
8
8
10
7
7
11
6
6
5
5
9
11c
11b
11a
3
2
4
1
1
step
step
C1
C2
C3
C4
C5
C6

Figure 15: The sedimentary texture of Lisar Trench. Unit 1: light brown alluvial deposits, layered, 90% grain; Unit 2: light gray lenticular deposits, more or less layered, 60% grain; Unit 3: dark brown alluvial deposits, layered, 5% grain; Unit 4: brown deposit, no layering, 60% grain; Unit 5: Light gray layered alluvial deposits, 90% grain; Unit 6: light brown alluvial deposits, layered, 75% grain; Unit 7: Layered gray to brown alluvial deposits, 35% grain; Unit 8: Layered light brown, deposits, 60% grain; Unit 9: Unlaminated light brown alluvial deposits, 40-90% grain; Unit 10: Unlaminated alluvial brown deposits, 50% grain; Unit 11: Layered dark brown alluvial deposits, 5% grain; Unit a11: Layered lenticular light brown deposits, 90% grain; Unit b11 and unit c11: lenticular light brown deposits, layered, 65% grain; Unit 12: Layered light brown to gray, deposits, 95% grain; Unit 13: top soil.

Table 2: Description of the sedimentary deposits of the segregated units in the main fault zone in the south wall of the Lisar Trench.

Description of Units in Lisar Trench

1	**Unit1:** alluvial deposit: ,mediom sorted,sub rounded,sub angular pebbles (20 per cent ,0.5-7cm) with clay and sand as matrix.
2	**Unit2:** alluvial deposit as lens,poorly sorted,sub rounded to rounded pebbles (20 per cent , 0.5 -10 cm) sandy matrix,add root plant.
3	**Unit3:** alluvial deposit: ,sub rounded pebbles(0.5-2 cm) clay as matrix- ,add the char.plant.
4	**Unit4:** colluvium wege, non- sorted,sub rounded to rounded,sub angular pebbles (25 per sent,0.5-7 cm) clay matrix.
5	**Unit5:** alluvial deposit,medium sorted,sub rounded to rounded pebbles (40 per cent, 0.5-7 cm) sany silty clay matrix,add the lichen.
6	**Unit6:** alluvial deposit,sub angular pebbles (30per cent ,0.5-10 cm) sandy silty clay matrix,same place add the limonite and root plant.
7	**Unit7:** alluvial deposit, non-sorted,sub rounded,sub angular pebbles (70 per sent ,0.5-30cm) clay silty sand matrix.
8	**Unit8:** alluvial deposit, poorly sorted,sub rounded pebbles (25 per sent , 0.5-7 cm) Bace matrix: clay , top matrix: sandy silty clay,add the root plant.
9	**Unit9:** alluvial deposit, poorly sorted,sub rounded pebbles (25 per cent ,0.5 -10 cm) sandy clay silt matrix,add the root plant and lichen.
10	**Unit10:** alluvial deposit, poorly sorted,sub rounded,sub angular pebbles (35 per cent, 0.5-10 cm) clay silty sandy matrix.
11	**Unit11:** alluvial deposit, (15 per cent, 0.5-1 cm) clay matrix,include some in layer lens gravel,biotorbination,add the root plant and lichen and char.sandy matrix.
11a	**Unit 11a:** alluvial deposit as lens, poorly sorted,sub rounded to sub angular pebbles (15 per cent,0.5-10 cm) clay sandy silt matrix.
11b	**Unit 11b:** alluvial deposit as lens, sub rounded to sub angular pebbles (6 per sent,0.2-2.5 cm) silty clay sand matrix,add the char.
11c	**Unit 11c:** alluvial deposit as lens, medium sorted,sub rounded to sub angular pebbles (6 per sent ,0.2-2.5 cm) silty clay sand matrix.
12	**Unit 12:** alluvial deposit, pebbles (40 per cent, 0.5-15 cm) Bace matrix: clay silt, top matrix: sandy silt,add the lichen.
13	**Unit 13:** Artificial

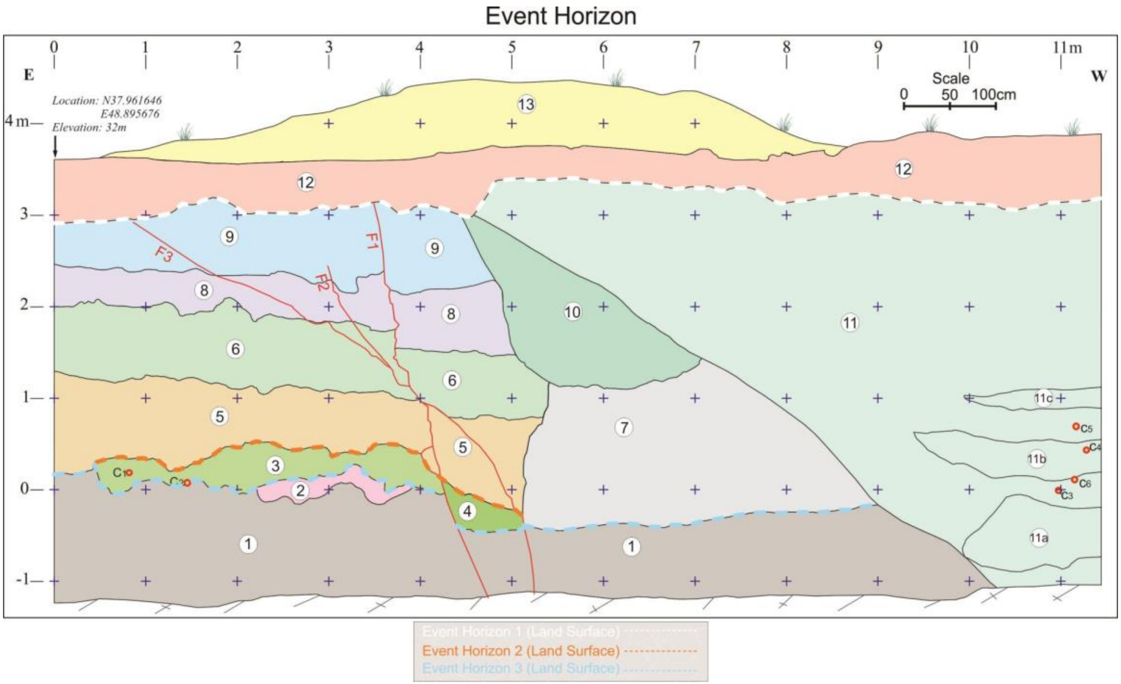

Figure 16: The event horizons of four paleoearthquakes in the main zone of the Astara fault, in the Lisar trench.

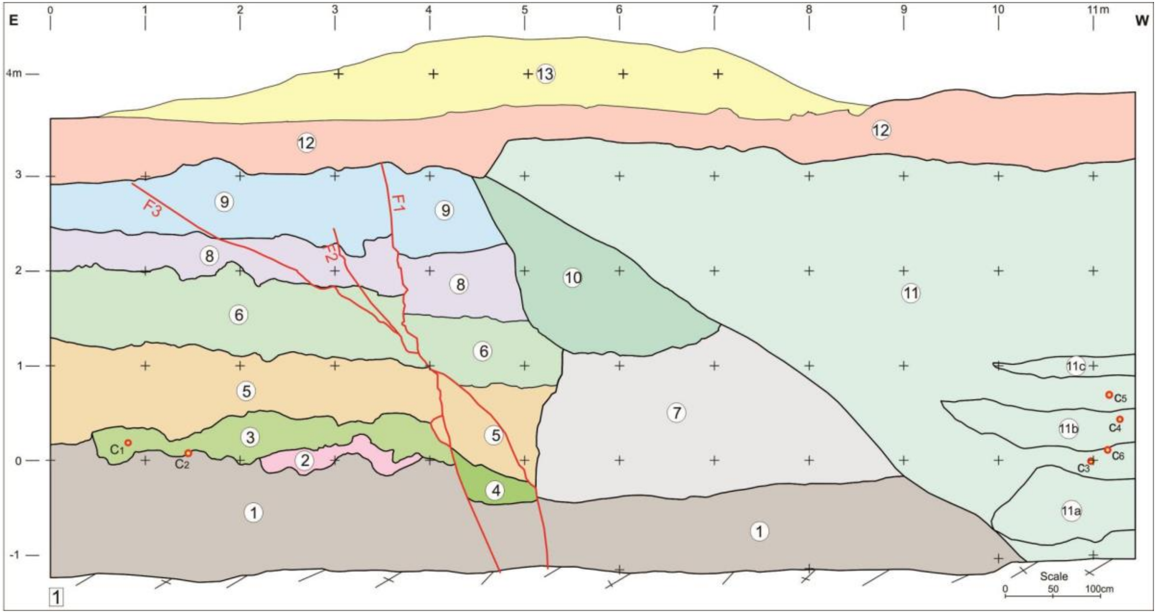

Figure 17: The layout of events in the present time.

3-3- Reconstruction of the identified events in Lisar trench

Using the Figure 17, by removing systematically the known sedimentary units, and reconstructing the unite on the basis of the maximum heights, we were able to reconstruct paleo-seismic events of course, this procedure must be start with removing the manmade soil (unit 13 in Figure 17), and continues until Figure 48.

By carrying out the reconstruction, it is possible to realize the height of the fault scarp at the time of the earthquakes, and finally, by applying the empirical relationships, to obtain the magnitude of paleo-earthquakes.

At the beginning of the reconstruction and identification of events in the Lisar trench, two methods have been used, due to the possibility of occurrence of both methods (Figure 21 & Figure 23 related to the first method; Figure 24 & Figure 25 related to the second method), although it seems that the first method of reconstruction is more likely to occur. From Figure 26 to Figure 48, the reconstructions are done by only one method and they are not different from each other.

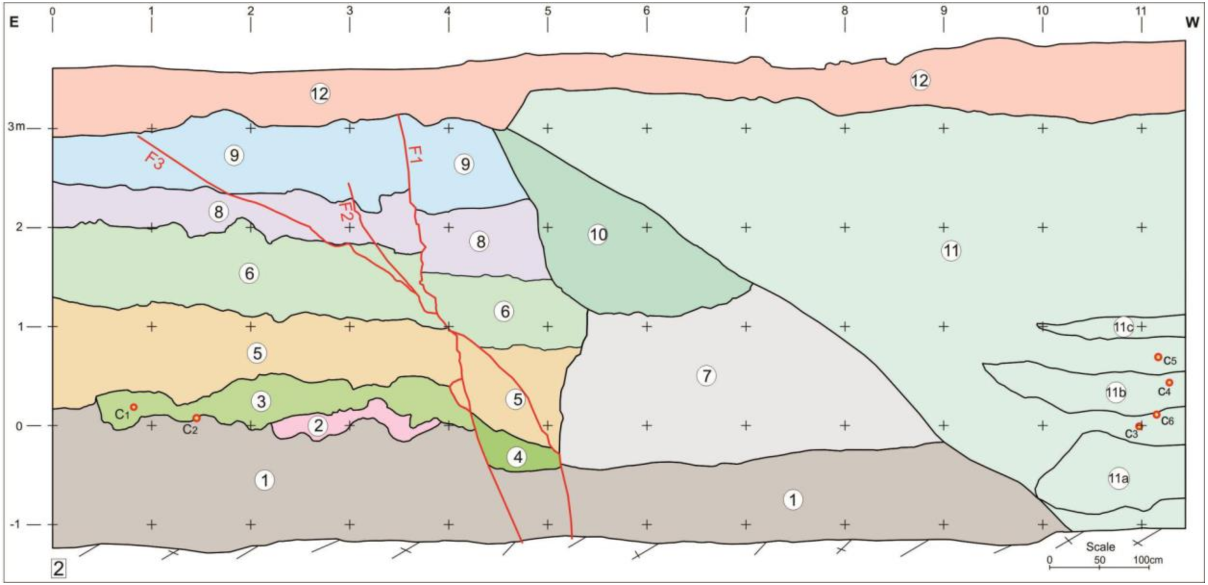

Figure 18: Reconstruction of events recorded in the southern wall of Lisar Trench, first step.

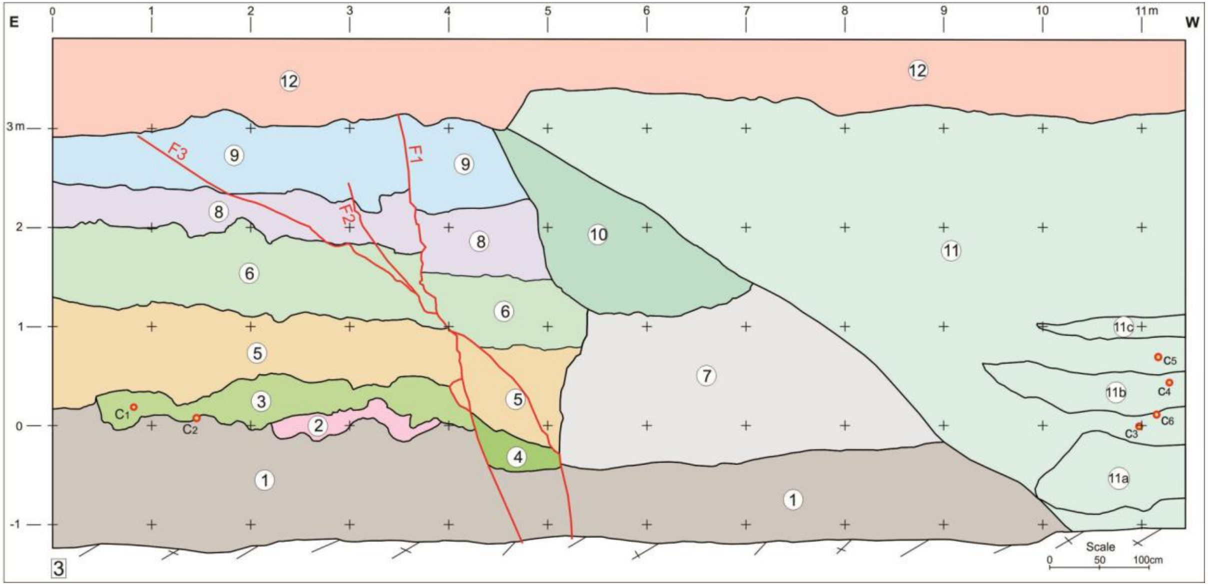

Figure 19: Reconstruction of events recorded in the southern wall of Lisar Trench, second step.

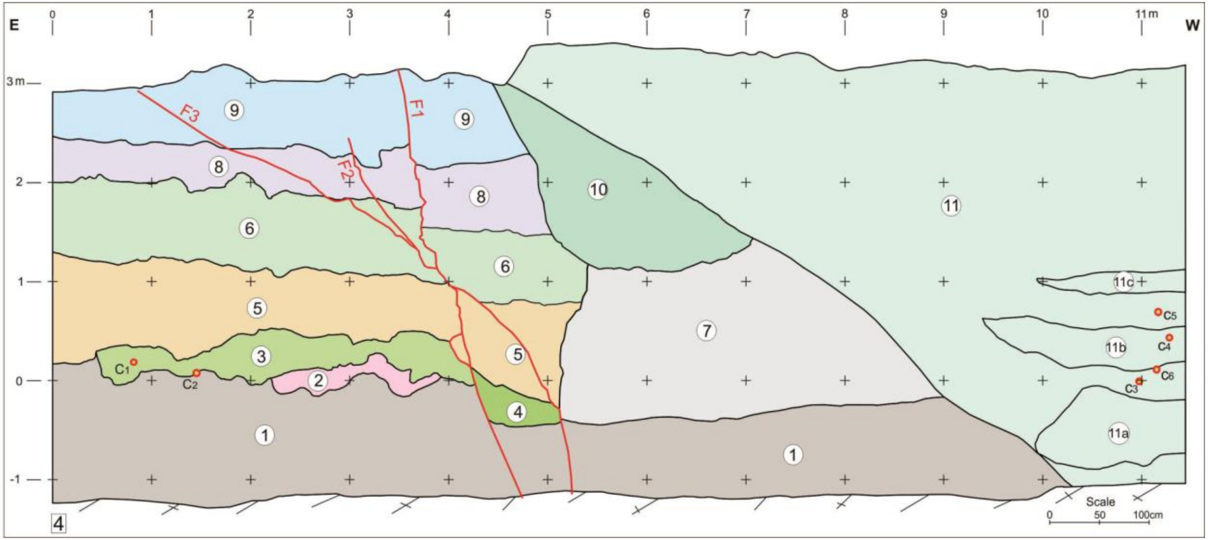

Figure 20: Reconstruction of events recorded in the southern wall of Lisar Trench, third step.

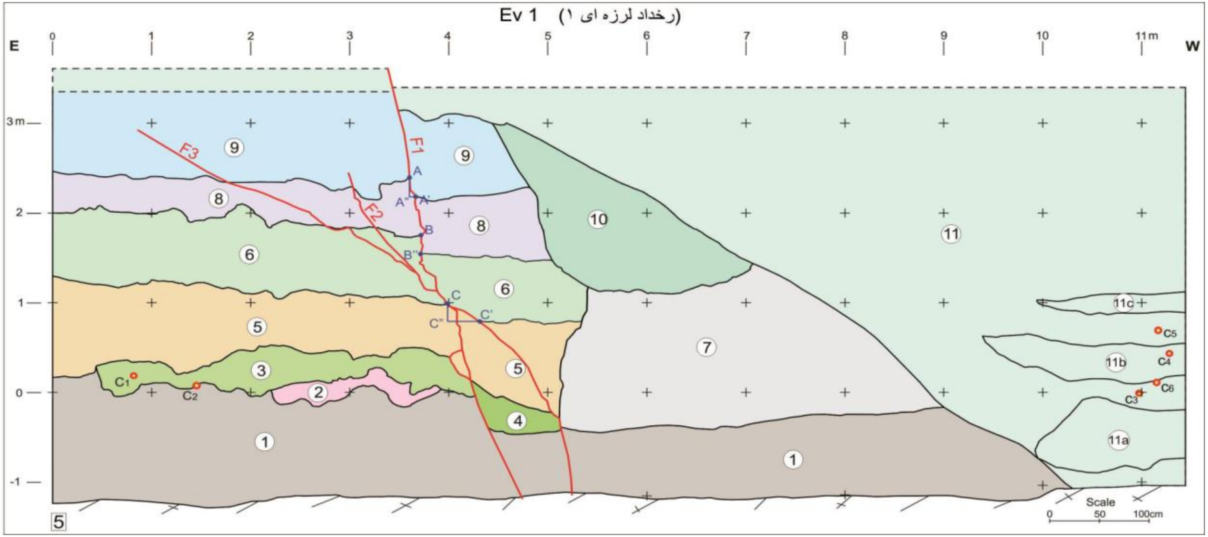

Figure 21: Reconstruction of events recorded in the southern wall of Lisar trench, fourth step (first method).

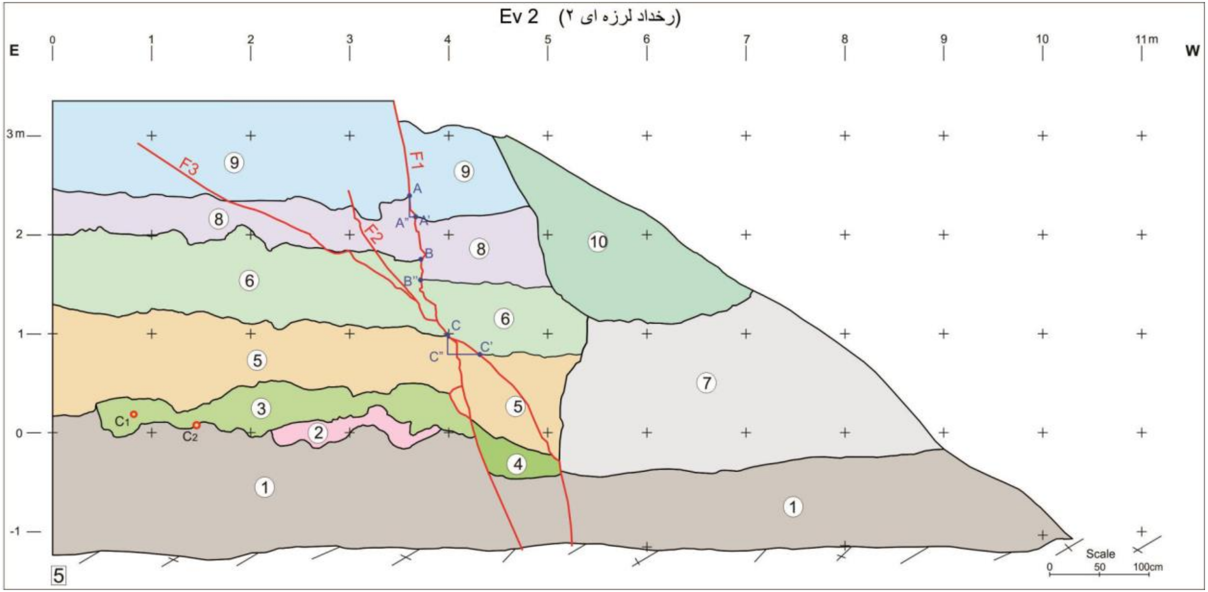

Figure 22: Reconstruction of events recorded in the south wall of Lisar trench, fifth step (first method).

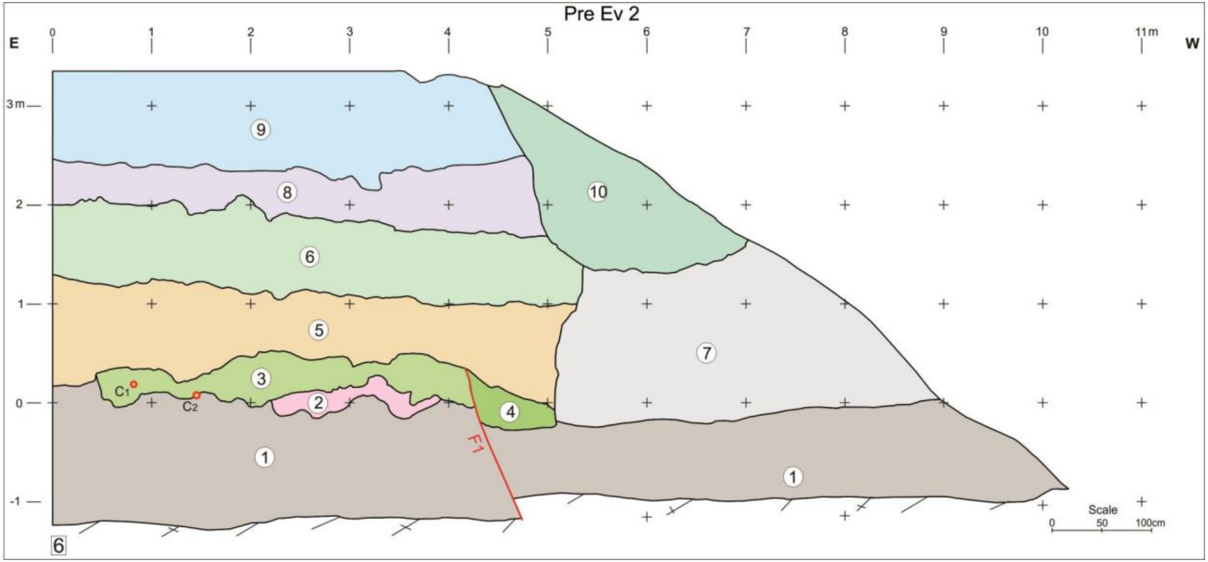

Figure 23: Reconstruction of events recorded in the southern wall of Lisar trench, sixth step (first method).

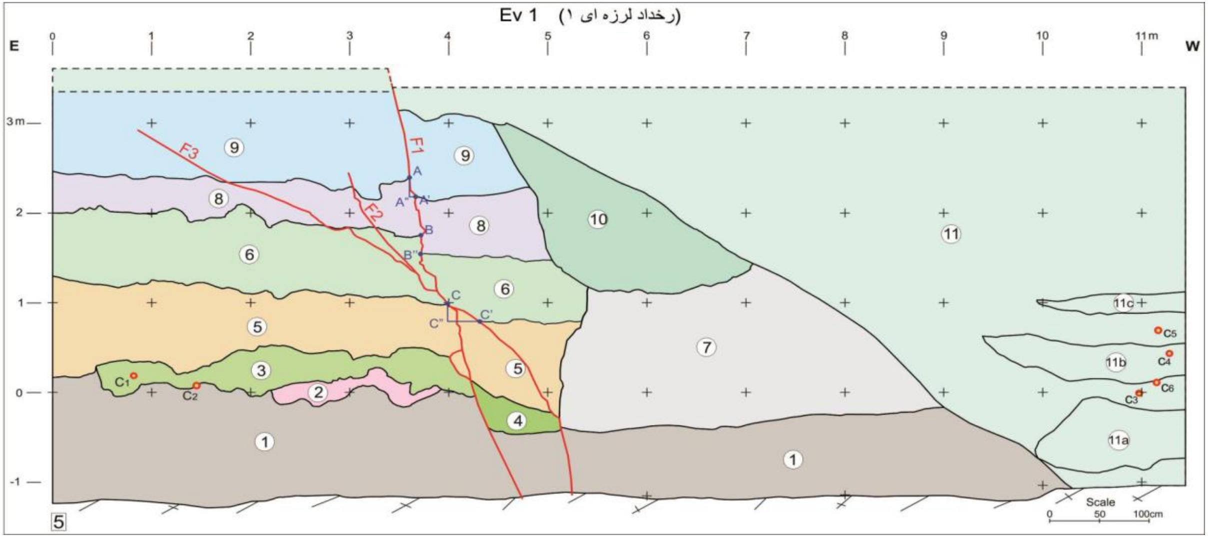

Figure 24: Reconstruction of events recorded in the south wall of Lisar trench, fourth step (second method).

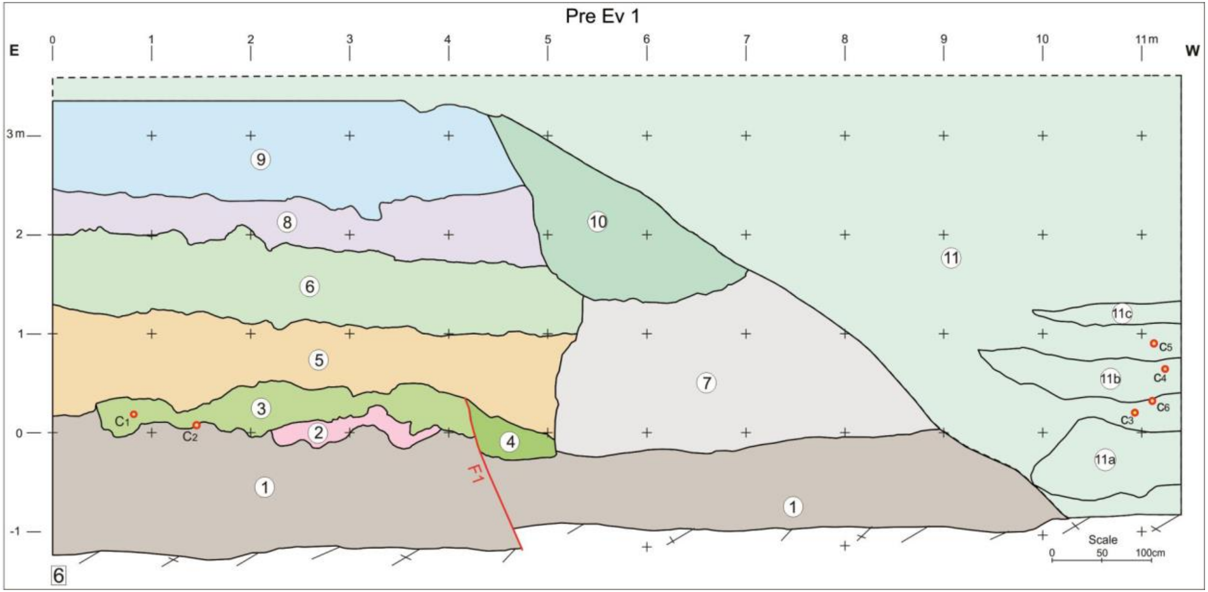

Figure 25: Reconstruction of events recorded in the southern wall of Lisar trench, fifth step (second method).

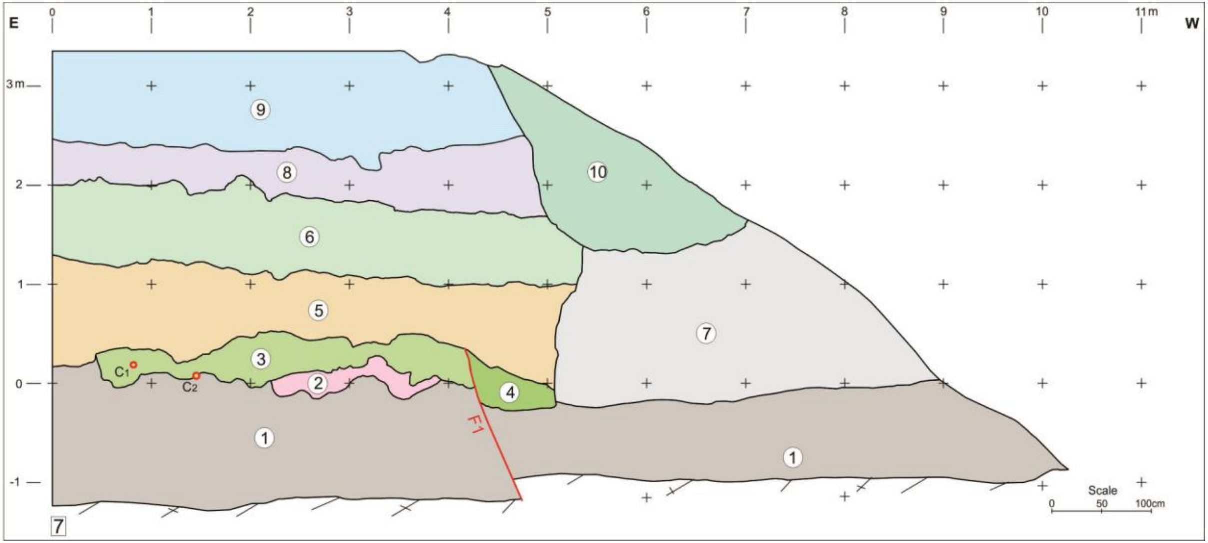

Figure 26: Reconstruction of events recorded in the southern wall of the Lisar trench, the sixth step.

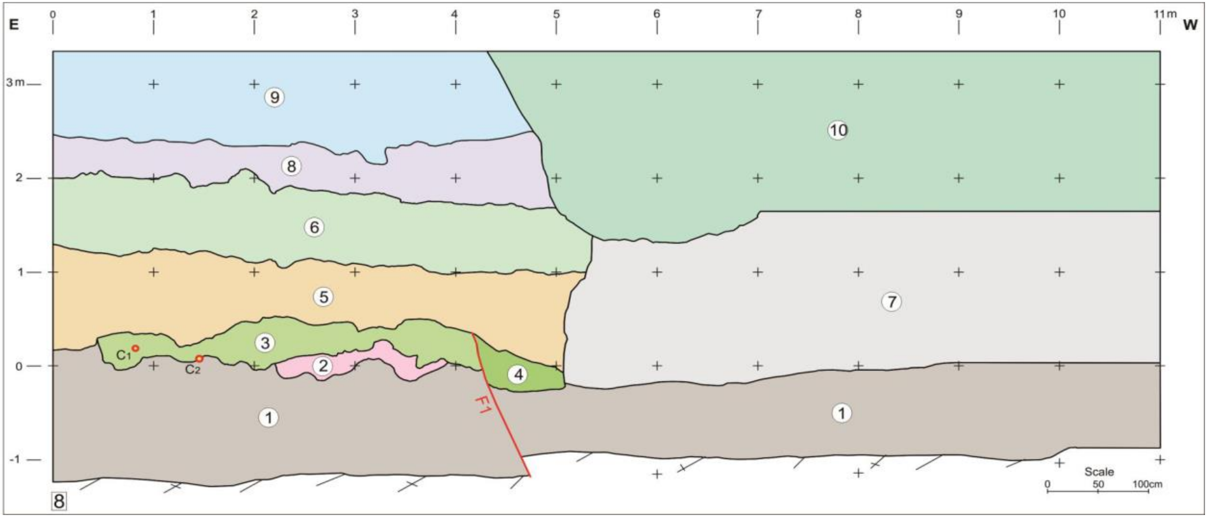

Figure 27: Reconstruction of events recorded in the southern wall of the Lisar trench, the seventh step.

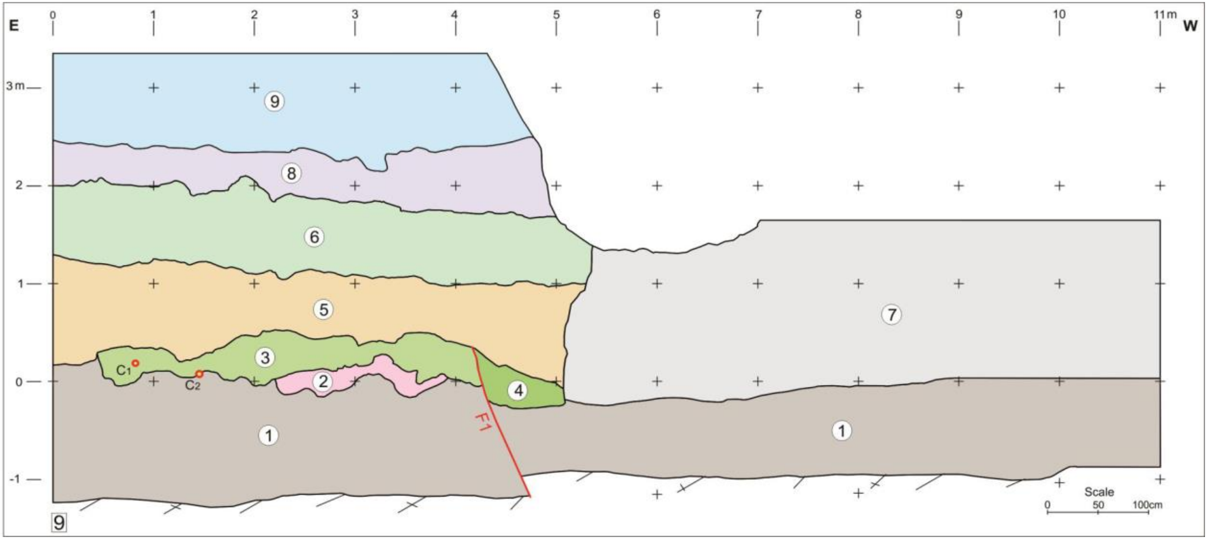

Figure 28: Reconstruction of events recorded in the southern wall of Lisar Trench, the eighth step.

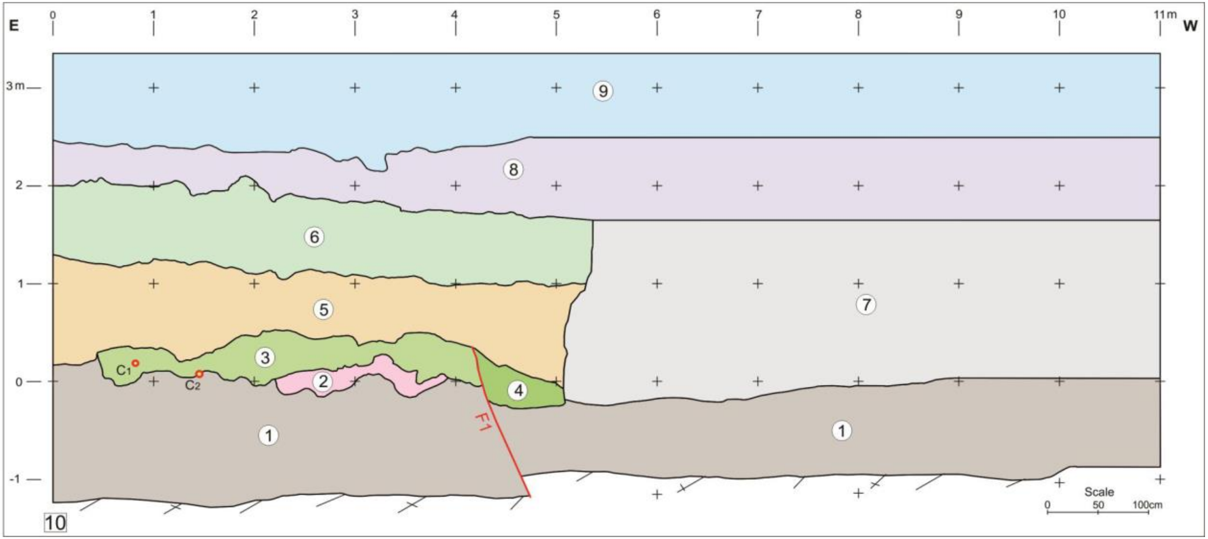

Figure 29: Reconstruction of events recorded in the southern wall of Lisar Trench, step nine.

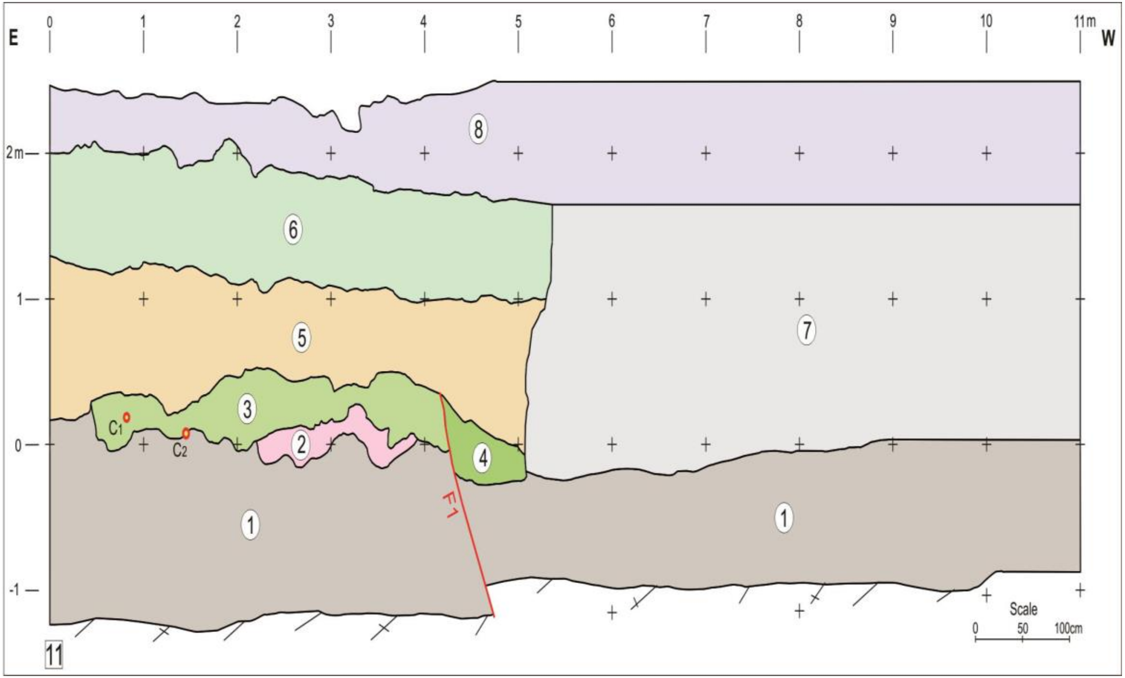

Figure 30: Reconstruction of events recorded in the south wall of Lisar Trench, 10th step.

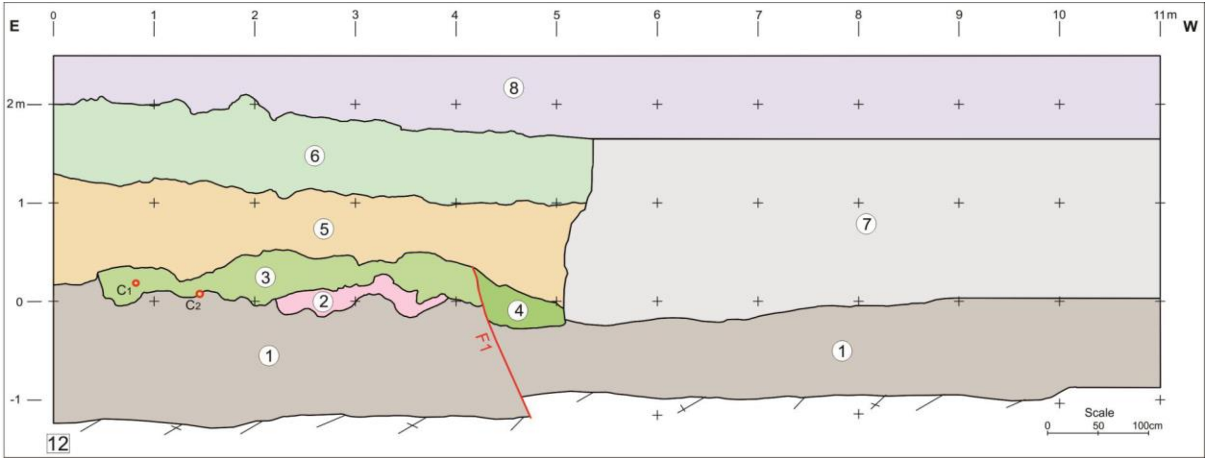

Figure 31: Reconstruction of events recorded in the southern wall of Lisar Trench, Step 11.

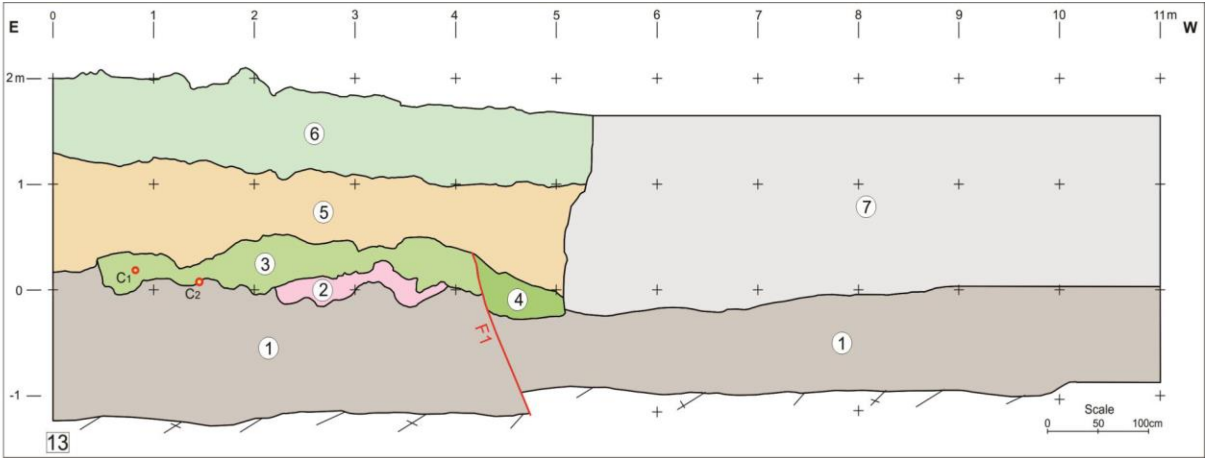

Figure 32: Reconstruction of events recorded in the southern wall of Lisar trench, twelfth step.

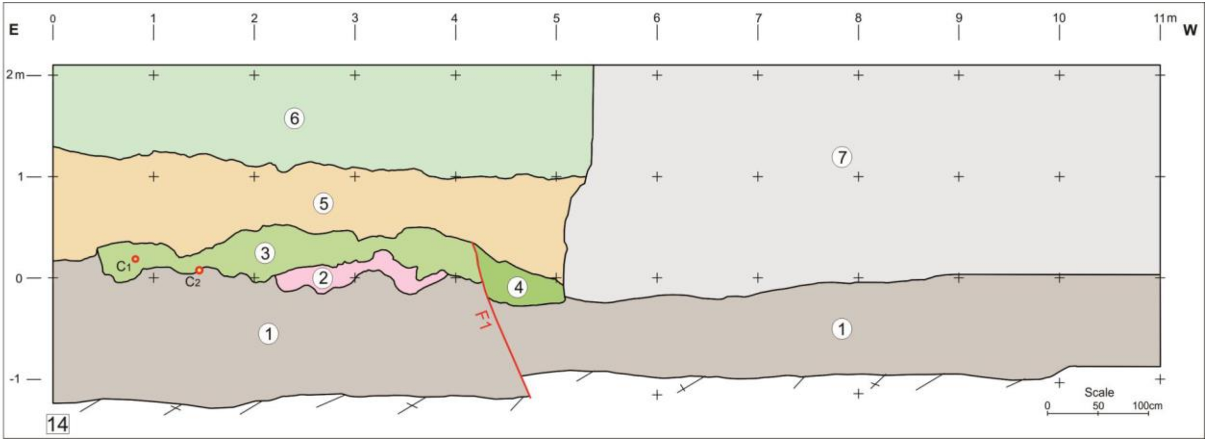

Figure 33: Reconstruction of events recorded in the southern wall of Lisar Trench, step 13.

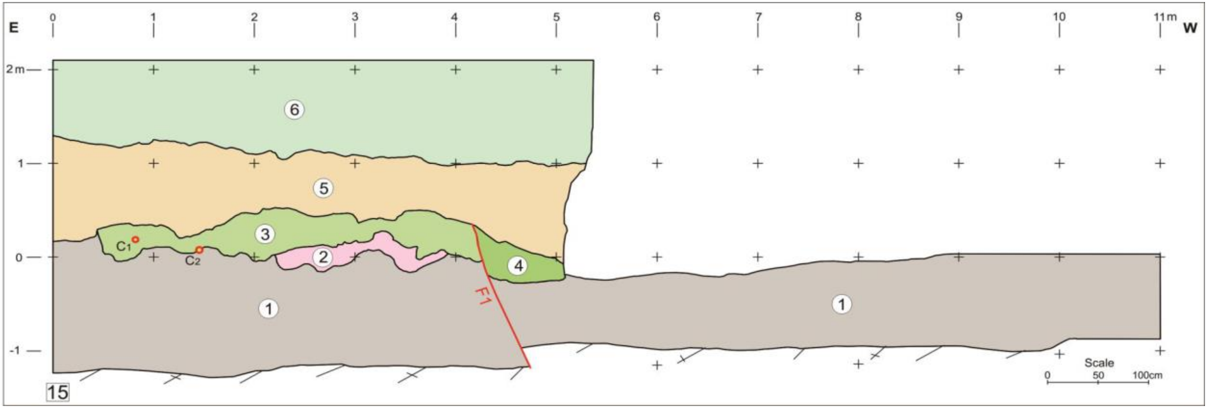

Figure 34: Reconstruction of events recorded in the southern wall of the Lisar trench, the fourteenth step.

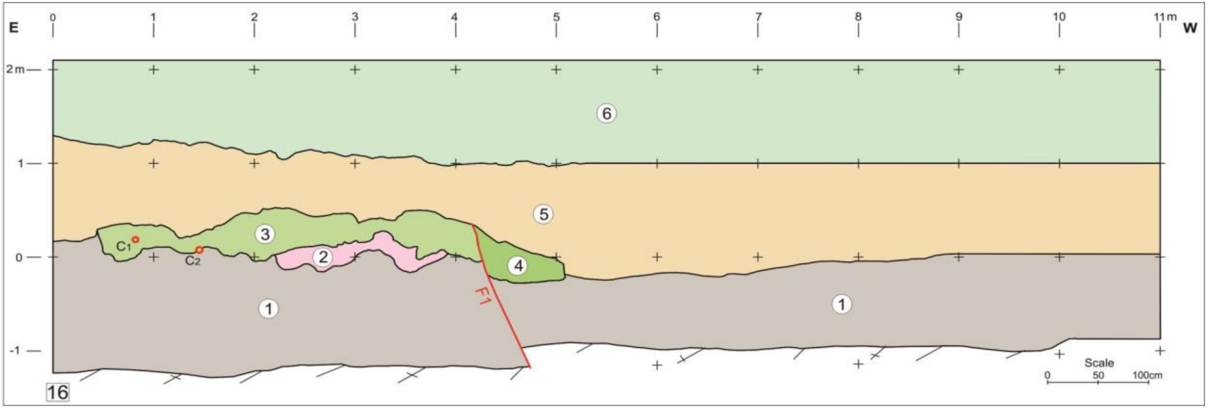

Figure 35: Reconstruction of events recorded in the southern wall of Lisar Trench, step 15.

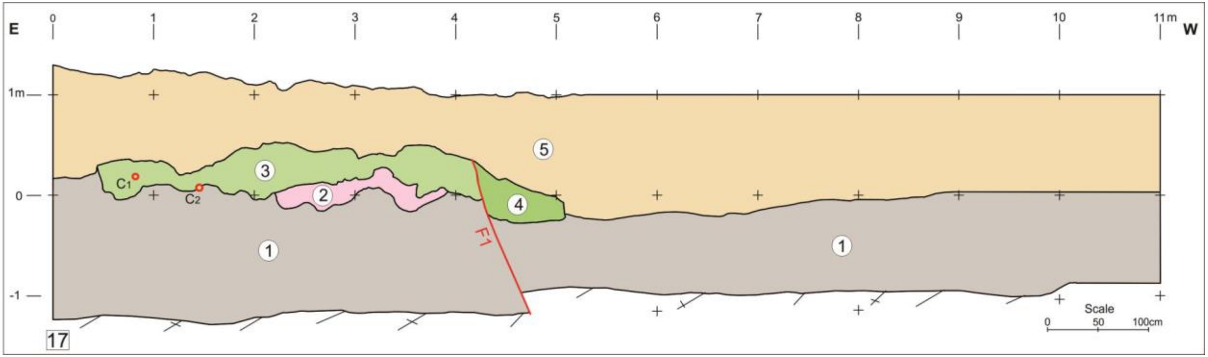

Figure 36: Reconstruction of the recorded events in the southern wall of the Lisar trench, the 16th step.

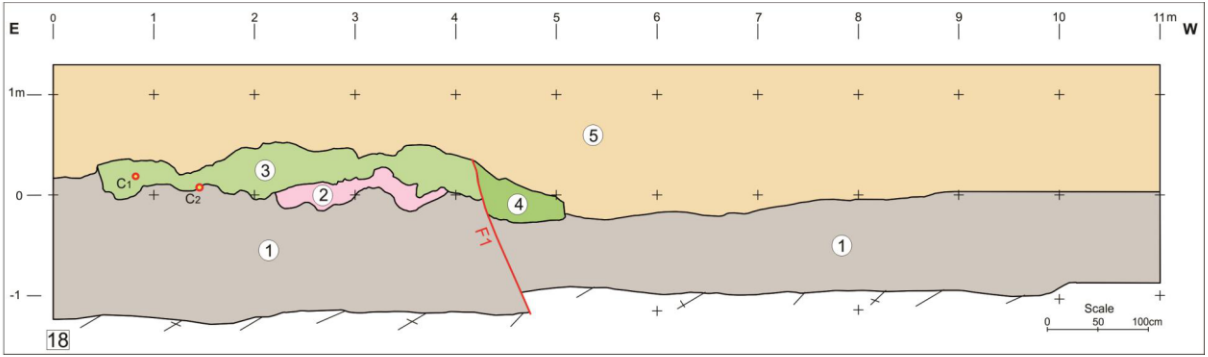

Figure 37: Reconstruction of events recorded in the southern wall of Lisar Trench, 17th step.

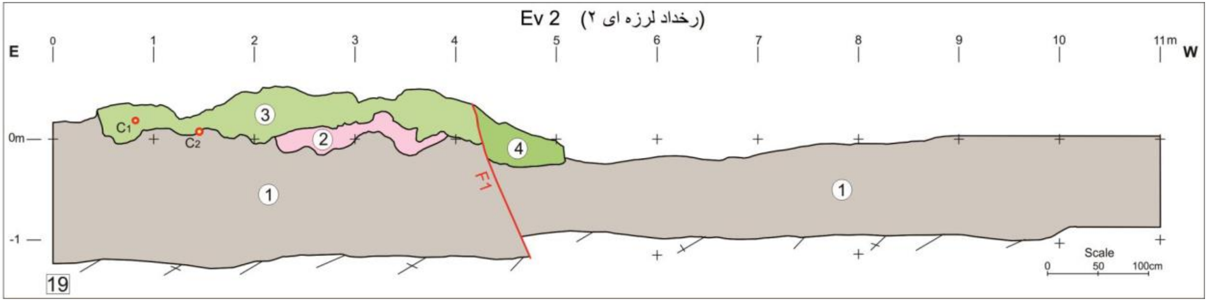

Figure 38: Reconstruction of events recorded in the southern wall of Lisar Trench, step 18. Display of units at the time of the second earthquake detected in this trench.

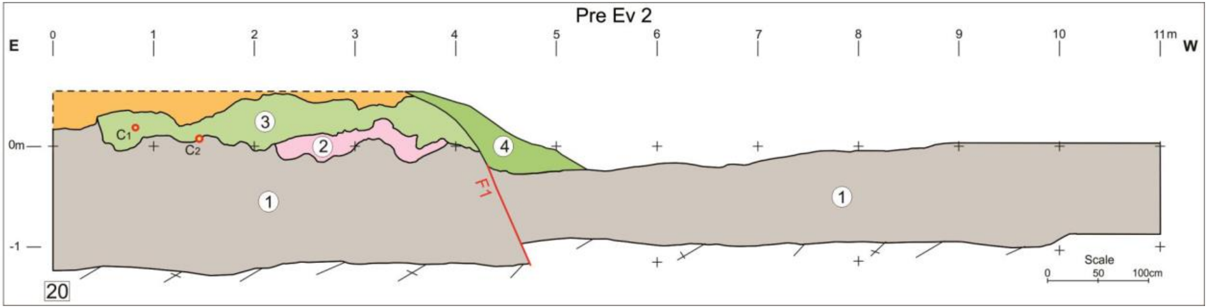

Figure 39: Reconstruction of events recorded in the southern wall of Lisar trench, 19th step. Display of the units in the time before the second earthquake detected in this trench.

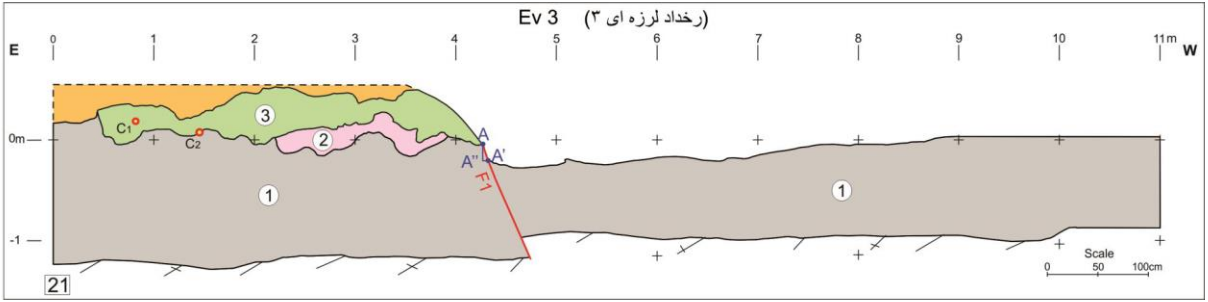

Figure 40: Reconstruction of events recorded in the southern wall of Lisar Trench, the 20th step. Showing the units at the time of the oldest earthquake detected in this trench and before the formation of the debris wedge.

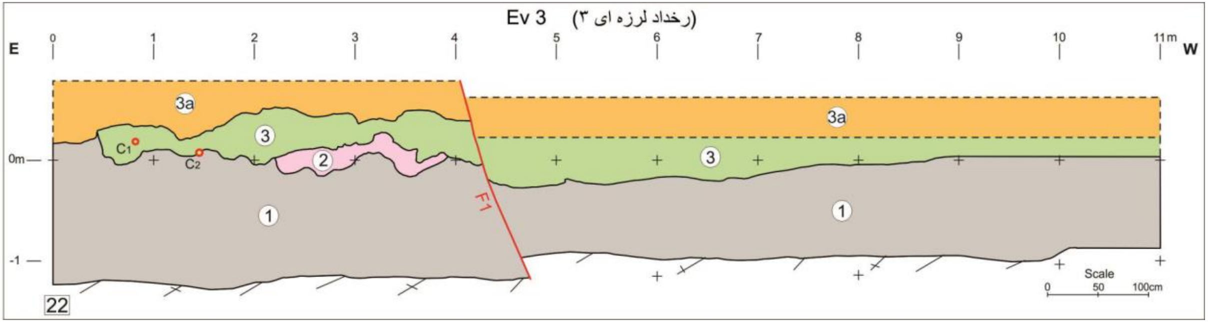

Figure 41: Reconstruction of events recorded in the southern wall of Lisar Trench, 21st step.

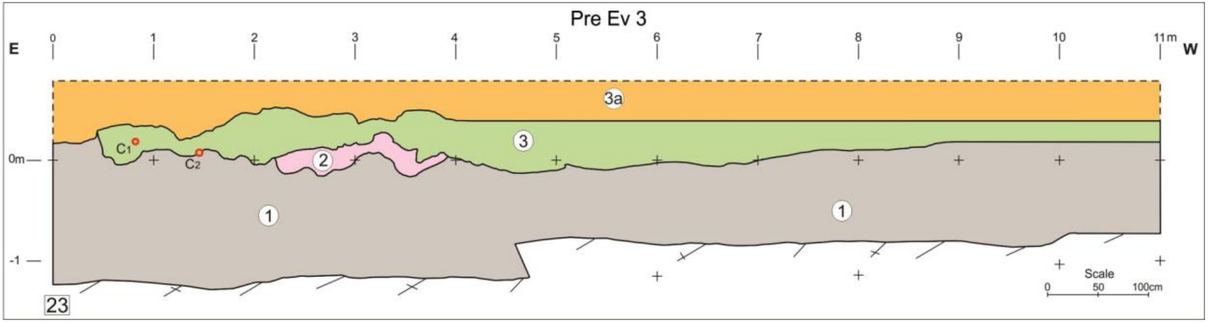

Figure 42: Reconstruction of events recorded in the southern wall of the Lisar trench, step twenty-two.

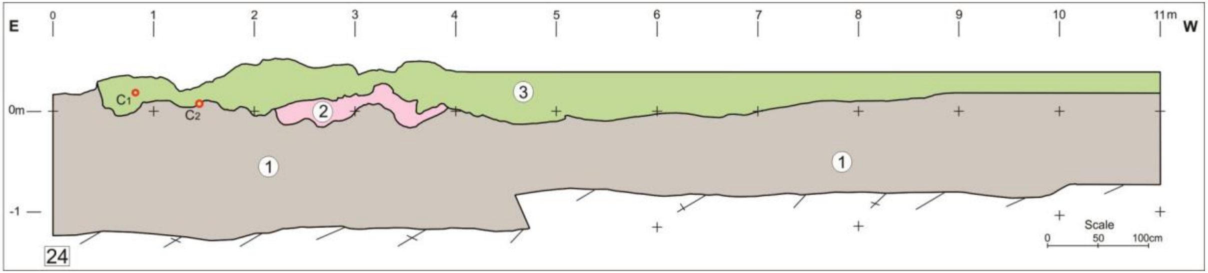

Figure 43: Reconstruction of events recorded in the southern wall of Lisar Trench, the twenty-third step.

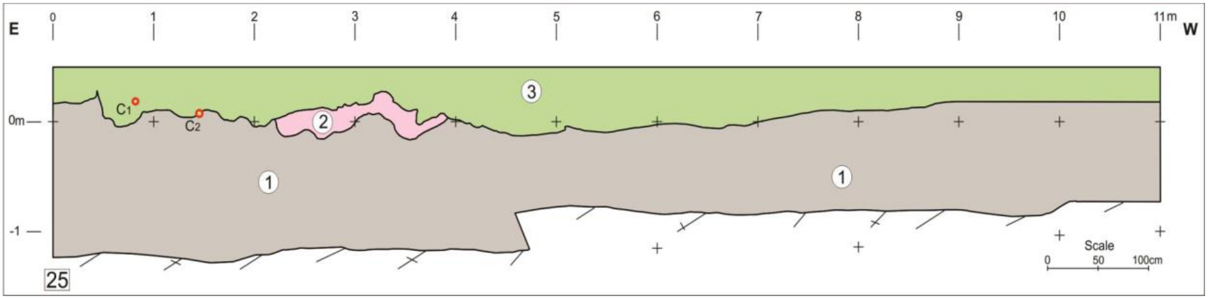

Figure 44: Reconstruction of events recorded in the southern wall of the Lisar trench, the twenty-fourth step. Showing the units in the time before the oldest earthquake detected in this trench.

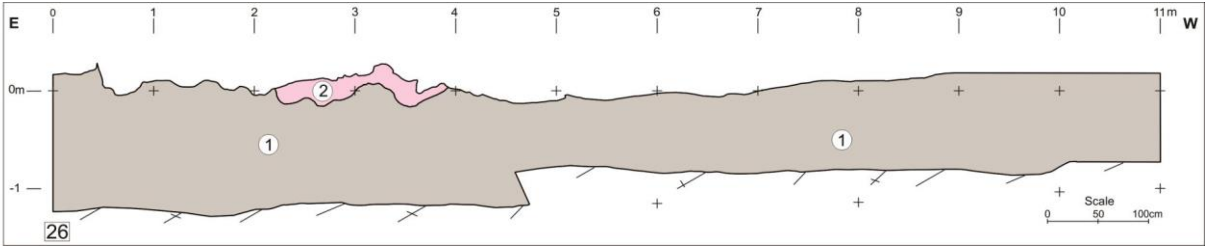

Figure 45: Reconstruction of events recorded in the southern wall of the Lisar trench, the twenty-fifth step.

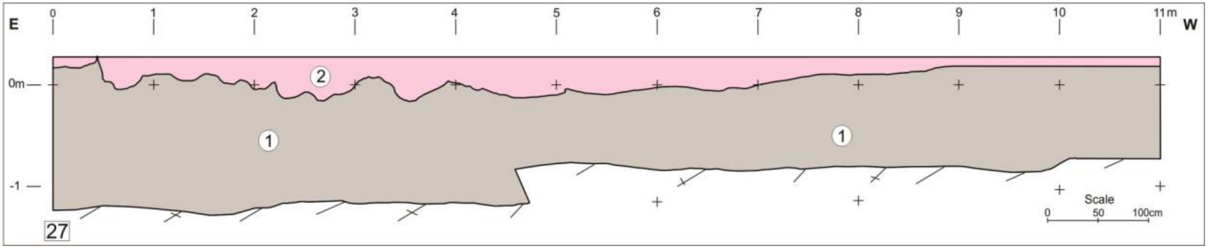

Figure 46: Reconstruction of events recorded in the southern wall of the Lisar trench, the twenty-sixth step.

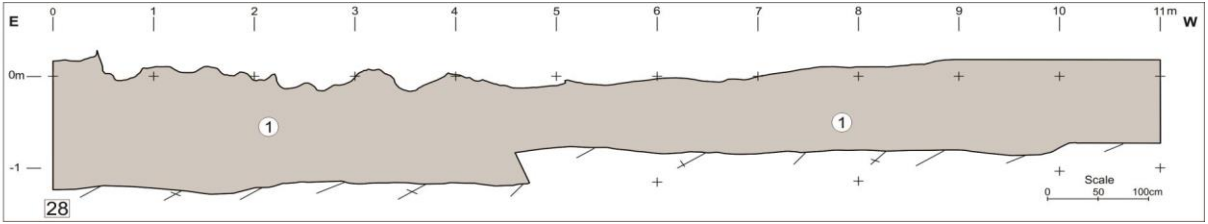

Figure 47: Reconstruction of events recorded in the southern wall of the Lisar trench, the twenty-seventh step.

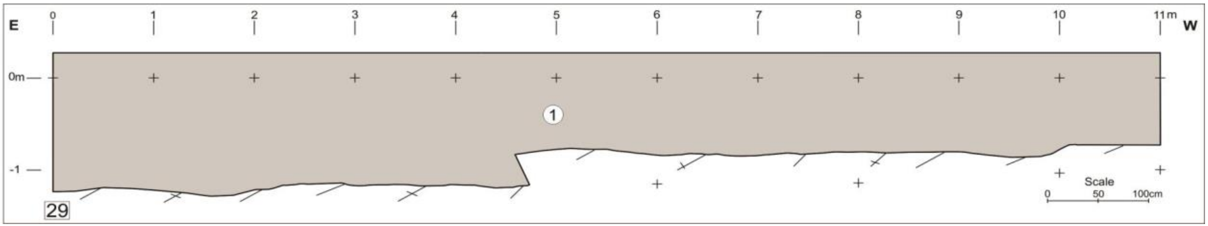

Figure 48: Reconstruction of events recorded in the southern wall of the Lisar trench, the twenty-eighth step.

3-4- Interpretation of identified paleoseismic events

In the identified youngest event by the first method (Figure 21; Event 1), the fault has hypothetically displaced layer 11. If we remove unit 11 (event 2), then units 5, 6 and 8 are approximately displaced normally 20 cm and since the fault has reached to the top of unit 9, it is possible unit 9, also displaced by the activity of this fault (Figure 21 to Figure 24; Table 5). In the second method, only one event has been identified, in which units 5, 6, 8, 9, and 11 were displaced by an apparently normal fault, and this faulting occurred on fault F1. The next event, which is considered as the third event in the first method and event 2 in the second method, has been identified due to the faulted colluvial wedge (Figure 38). The last event identified in the Lisar trench is supposed to be normal displacement in unit 1, and the presence of a colluvium wedge next to unit 3, which was created due to the oldest event. Therefore, one of the constituent units of the colluvial wedge is unit 3 (Figure 15 & Table 2). The thickness of unit 3a is obtained according to the average thickness of the colluvial wedge. By reconstruct on of units 3 and 3a, we reconstructed the faulting of these units as well (Figure 49).

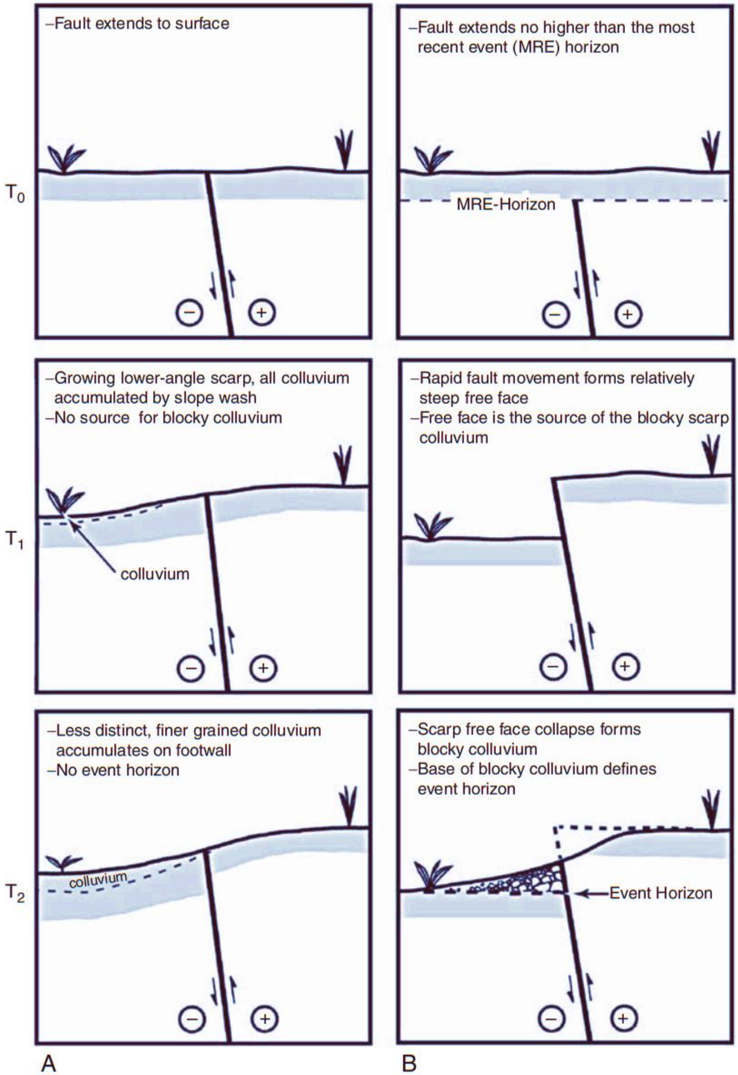

Figure 49: Stratigraphic comparison caused by strike-slip fault movements, creep movement (a) instantaneous seismic movement (b), time elapsed from T0 to T2 (Lienkaemper et al. 2002) With

regards to figure b at time T1 and T2, it can be seen that the formation of the colluvial wedge is directly related to the collapse of the fault scarp, therefore, in the reconstruction of the paleoseismological log by removing the colluvial wedge, it is necessary to give a height equal to the average diameter of the wedge to the fault scarp.

3-5- The evidence of identified paleoearthquakes

The detection of a colluvial wedge cross-cutting in the trench is evidence of the occurrence of at least two paleoearthquakes in this trench, while further studies indicate 3 to 4 paleoearthquake in this same trench. As mentioned earlier, there are two possibilities for reconstruction of Lisar trench. In the first method, unit 11 was faulted by an event younger than the event that displaced units 9, 8, 6, and 5. But in the second method, the existence of unit 11 is attributed before to the faulting of unit 9, so in the same proportion that units 8, 6, and 5 are displaced, we apply this displacement to units 9 and 11 and perform the reconstruction. Table 3 & Table 4 show the events detected in Lisar Trench and evidence of paleoearthquakes.

3-6- Estimation of paleoearthquakes magnitude identified in Lisar trench

The values of vertical displacement in each paleoearthquake are listed in Table 5 to Table 7. The measurements were made by CorelDraw software and include the values of vertical displacement on the fault plane (Vf) and in the vertical axis (V) in each event.

Estimates of displacement and magnitude of paleoearthquakes are given in Table 3-6, and based on rake values obtained by Kaveh Firouz et al. (2013) and using the relations of Wells and Coppersmith (1994).

To estimate magnitude based on empirical relationships, we must first calculate the amount of net slip for each seismic event. Therefore, the amount of net slip is obtained from the following relationship:

$$\boldsymbol{Net\ Slip = AD = V_{Tr}/SinR}$$

V_{Tr} is the total vertical displacement visible in the trench (Table 5 & Table 6), AD is the amount of net slip, R is the value of Rake. Following estimating the value of the net slip of the fault in each identified event, and by using the Wells and Coppersmith (1994) relation, it is possible to estimate the magnitudes of the oldest known earthquakes in the trench.

$$F_{Strike\ Slip} = M_W = 7.04 + 0.89 \log{(AD)}$$

$$F_{General} = M_W = 6.93 + 0.82 \log{(AD)}$$

Table 3: The evidence of the seismic event horizon identified (by the first method) in the main fault zone in the southern wall of the Lisar trench.

Event	**Event Horizon**	**Evidences**
Event 1	Top of unite 11	Truncation of unit 9 by fault F1
Event 2	Top of unite 9 and 10	Truncation of unit 5, 6, 8 and 9 by fault F1
Event 3	Top of unite 1 and 3	Truncation of colluvial wedge (unit 4)
Event 4	Top of unite 1	Formation of colluvial wedge (unit 4), vertical displacement of unit 1, by fault F1

Table 4: Evidence of seismic event horizon identified (by the second method) in the main fault zone in the southern wall of the Lisar trench.

Event	**Event Horizon**	**Evidences**
Event 1	Top of unite 11	Truncation of unit 9 by fault F1
Event 2	Top of unite 1 and 3	Truncation of colluvial wedge (unit 4)
Event 3	Top of unite 1	Formation of colluvial wedge (unit 4), vertical displacement of unit 1, by fault F1

Table 5: Vertical displacement values at the time of the second earthquake event, measurements were made on log number 5.

Event 2 or Event1				
V_f	AA'	BB'	CC'	Total
Measurement (cm)	21	–	37.38	58.38
V	AA''	BB''	CC''	Total
Measurement (cm)	20.09	19.62	18.69	58.4

Table 6: Vertical displacement values at the time of the last earthquake event, measurements were made on Log No. 21.

Event 4		
V_f	AA'	Total
Measurement (cm)	16.3	16.3
V	AA''	Total
Measurement (cm)	15.4	15.4

Table 7: Estimated displacement values and magnitudes of paleoearthquakes indentified in the Lisar trench.

Event	Event Horizon	V_f (m)	AD (min)	AD (mean)	AD (max)	M_W (AD min) F_{SS}	M_W (AD min) F_G	M_W (AD $mean$) F_{SS}	M_W (AD $mean$) F_G	M_W (AD max) F_{SS}	M_W (AD max) F_G	F_{SS} (Total)	F_G (Total)
1	Top of Unit 11	0.584	0.3	0.13	0.08	6.57	6.5	6.25	6.2	6.06	6.03	6.29	6.24
2	Top of Unit 3 & 1	–	–			–	–	–	–	–	–		
3	Top of Unit 1	0.154	0.08	0.03	0.02	6.06	6.03	5.68	5.68	5.52	5.53	5.75	5.74

Chapter four

CONCLUSION

The Field studies along the Astara fault indicating different geomorphological, indices such as various amount of right- lateral river displacements, shutter ridges, etc. The main purpose of this study focused on Paleoseismological investigations on the southern segment of the Astara fault system in the Lisar trench in western coast of the South Caspian Basin.

The results show that the paleoearthquakes are probably younger than 30.000 years ago, and on the basis of local sedimentation rate of the trench, the youngest earthquakes may occur 5,000 years ago with magnitude 6.24. The estimated magnitude for oldest event (~ 30.000 years ago) is around 5.74.

References:

Ambraseys, N.N. &Melville, C.P., 1982, A History of Persian Earthquakes, Cambridge University Press, 240 pp.

Aziz Zanjani, A., Ghods, Ab., Sobouti, F., Bergman, E., Mortezanejad, Gh., Priestley, K., Madanipour, S. 2013, Seismicity in the western coast of the South Caspian Basin and the Talesh Mountains. Geophysical Journal International. doi: 10.1093/gji/ggt299.

Berberian, M. & King, G. C. P., 1981, Towards a palaeogeography and tectonic evolution of Iran, Can. J. Earth Sci., 18, 210 – 265.

Berberian, M. 1976, Contribution to the Seismotectonics of Iran (Part 2). Geological Survey of Iran, Rep. No. 39, 518 P.5 Maps. 259 Figures.

Berberian, M., 1983, The southern Caspian: a compressional depression floored by a trapped, modified oceanic crust, Can. J. Earth Sci., 20, 163– 183.

Berberian,M. & Yeats, R.S., 1999, Patterns of historical earthquake rupture in the Iranian plateau, Bull. seism. Soc. Am., 89, 120–139.

Djamour, Y., Vernant, P., Nankali, H.R. & Tavakoli, F., 2011, NW Iraneastern Turkey present-day kinematics: results from the Iranian permanent GPS network, Earth planet. Sci. Lett., 307, 27–34.

England, P & Molnar, P, 1990, Right-lateral shear and rotation as the explanation for strike-slip faulting in eastern Tibet, Nature. 344, 140-142.

Hessami, K., Jamali, F. & Tabassi, H., 2003, Major Active Faults of Iran (map), scale 1:2,5000,000, Ministry of Science, Research and Technology, International Institute of Earthquake Engineering and Seismology.

Hessami, K., Pantosi, D., Tabassi, H., Shabanian, E., Abbassi, M., Feghhi, K., Solaymani, S., 2003, Paleoearthquakes and slip rates of the North Tabriz Fault, NW Iran: preliminary results, Ann. Geophys., 46, 903–915.

Jackson, J., Priestley, K. & Berberian, M., 2002, Active tectonics of the South Caspian Basin, Geophys. J. Int., 148, 214–245.

Kaveh Firouz, A., Nazari, H., Ghorashi, M., Halaj Neyshaburie, M., Einali, A., Roozegar, R., Mirzaei, M., Mohammadi Vizheh, M., Sobouti, F., Asaadi, V., Razavi, A., Baharfirouzi, Kh., Karimi Bavandpour, A., Arefipour, S., Roustaei,

M. 2013, Morphotectonic Map of The Talesh Mountains, Geological survey of Iran.

Kaveh Firouz, A., Nazari, H., Ghorashi, M., Mohammadi Vizheh, M., Sobouti, F., Asaadi, V., Razavi, A., Baharfirouzi, Kh., Karimi Bavandpour, A., Arefipour, S., Roustaei, M. 2013, Sismotectonic Map of The Talesh Mountains, Geological survey of Iran.

Kurushin, R.A., Bayasgalan, A., Olziybat, M., Enhtuvshin, B., Molnar, P, Bayarsayhan, Ch., Hudnut, K.W. & Lin, J., 1997, The surface rupture of the 1957 Gobi-Altay, Mongolia, earthquake, Geol. Soc. Am. Special Paper# 320.

Lienkaemper, J. J., Dawson, T. E., Personius, S. F., Seitz, G. G., Reidy, L. M., and Schwartz, D. P. 2002, A record of large earthquakes on the southern Hayward fault for the past 500 years. Bull. Seis. Soc. Am. 92(7), 2637–2658.

Mangino, S., and Priestley, K., 1998, The crustal structure of the southern Caspian region: Geophysical Journal International, v. 133, p. 630–648, doi: 10.1046/j.1365 246X.1998.00520.x.

McKenzie, D.P., 1972, Active tectonics of the Mediterranean region: Geophysical Journal of the Royal Astronomical Society, v. 30, p. 109–185.

Nazari, H. 2006, “Analyse de la tectonique récente et active dans l’Alborz Central et la région de Teheran: « Approche morphotectonique et paléoseismologique »”. Ph.D. thesis, Univ. of Montpellier II, France.

Nazari, H., Ghorashi, M., Talebian, M., 2013. seismotectonic map of the NW Iran, Scale 1:750000, GSI.

Nazari, H., Kaveh-F., A., Ensani, M.R., Bahar-F., Kh., Shokri, M.A., Karimi-B., A., Mohammadi-V., M., Sabouti, F., Asadi, V., Razavi, A., 2014- Possible fog wave in the south of Caspian due to a large earthquake. Proceedings of the 16th Iran Geophysics Conference, 223 (3), page 1-3.

Nazari, H., Ritz, J.-F., Walker, R.T., Salamati, R., Rizza, M., Patnaik, R., Hollingsworth, J., Alimohammadian, H., Jalali, A., Kaveh Firouz, A., Shahidi, A. 2014, Palaeoseismic evidence for a medieval earthquake, and preliminary estimate of late Pleistocene slip-rate, on the Firouzkuh strike-slip fault in the Central Alborz region of Iran. Journal of Asian Earth Sciences. 82, 124–135.

Priestley, K., Baker, C.&Jackson, J., 1994, Implications of earthquake focal mechanism data for the active tectonics of the South Caspian Basin and surrounding regions, Geophys. J. Int., 118, 111–141.

Reilinger, R., et al. 2006, GPS constraints on continental deformation in the Africa Arabia-Eurasia continental collision zone and implications for the dynamics of plate interactions, J. Geophys. Res., 111, B05411

Tsukuda, T., 1985, Long term seismic activity and present microseismicity on active faults in southwest Japan. Earthquake Pred. Res., 3:253-284.

Vernant, P. et al., 2004c, Deciphering oblique shortening of central Alborz in Iran using geodetic data, Earth planet. Sci. Lett., 223, 177–185.

Vernant, P., et al., 2004a, Contemporary crustal deformation and plate kinematics in Middle East constrained by GPS measurements in Iran and northern Iran, Geophys. J. Int., 157, 381–398.

Vernant, P., Nilforoushan, F., Hatzfeld, D., Abassi, M.R., Vigny, C., Masson, F., Nankali, H., Martinod, J., Ashtiani, A., Bayer, F., and Chery, J., 2004b, Present-day crustal deformation and plate kinematics in the Middle East constrained by GPS measurements in Iran and northern Oman: Geophysical Journal International, v. 157,

p. 381–398, doi: 10.1111/j.1365-246X.2004.02222. x.

Yeats, R., Sieh, K., & Allen, C., 1997, The Geology of Earthquakes: Oxford University Press.